

Spring 2015

# Thermodynamic Considerations in Molten Salt Electrolysis for Rare Earth Metals

Arwin Gunawan

*Montana Tech of the University of Montana*

Follow this and additional works at: [http://digitalcommons.mtech.edu/grad\\_rsch](http://digitalcommons.mtech.edu/grad_rsch)



Part of the [Metallurgy Commons](#)

---

## Recommended Citation

Gunawan, Arwin, "Thermodynamic Considerations in Molten Salt Electrolysis for Rare Earth Metals" (2015). *Graduate Theses & Non-Theses*. 22.

[http://digitalcommons.mtech.edu/grad\\_rsch/22](http://digitalcommons.mtech.edu/grad_rsch/22)

This Thesis is brought to you for free and open access by the Student Scholarship at Digital Commons @ Montana Tech. It has been accepted for inclusion in Graduate Theses & Non-Theses by an authorized administrator of Digital Commons @ Montana Tech. For more information, please contact [sjuskiewicz@mtech.edu](mailto:sjuskiewicz@mtech.edu).

# THERMODYNAMIC CONSIDERATIONS IN MOLTEN SALT ELECTROLYSIS FOR RARE EARTH METALS

by  
Arwin Gunawan

A thesis submitted in partial fulfillment of the  
requirements for the degree of

Master of Science in Metallurgical and Materials Engineering

Montana Tech  
2015



## Abstract

Many applications utilize rare earths as a part of their essential composition, such as: Ni-MH batteries, glass screen, magnets, fluorescent lightning, etc. These reactive elements are normally found as an oxide compound due to their affinity with oxygen. Their oxide formation exhibits a high standard free energy, which make them really stable. Consequently, extracting rare earths cannot be easily done with a simple acid-base reaction.

It has been known that there are two reduction ways to extract rare earth, metallothermic reduction and molten salt electrolysis process. Metallothermic method is determined by standard free energy formation, melting point, boiling point, vapor pressure, viscosity, and density. As for molten salt electrolysis, it is not only determined with those factors, but also a decomposition potential. Molten salt or fused salt is used as an electrolyte, because it has an excellent electric conductivity, heat capacity, and can also act as a solvent.

This work presents a comprehensive study on thermodynamic considerations of molten salt electrolysis for rare earth metals. Related publications' results are analyzed and summarized. It reveals that a mixture of molten salts can help reduce the melting point (at its eutectic point) and increase their electric conductivity. Furthermore, rare earth fluoride as a solvent can help increase the rare earth oxide solubility as the feed, while alkali metals exhibit a contrast result. A higher temperature also result in higher solubility. In chloride molten salt electrolysis, a stable divalent ion will be produced and result in a low current efficiency. Fluoride molten salt electrolysis has higher current efficiency than the chloride system, yet it requires more energy consumption due to a higher decomposition potential in fluoride system.

E-pO<sup>2-</sup> diagram was constructed, modeled and implemented for providing essential information in the reduction process of rare earths by using STABCAL program. This work selects neodymium in a 75mole%LiF-25mole%NdF<sub>3</sub> system to produce neodymium by molten electrolysis at 750°C. E-pO<sup>2-</sup> diagram showed the value of the decomposition potential of Nd, which is -5.08 volts calculated from Kubaschewski databases and -4.98 volts calculated from HSC databases. This is confirmed with the similar decomposition potential determined by V.A. Grebnev and V.P. Dmitrienko (2007) experiment that is 4-8 volt using similar conditions. At 5.5volts applied potential, the E-pO<sup>2-</sup> diagram also showed a tendency of Nd metal to decompose rather than Li metal (higher driving force) with an overvoltage ( $\eta$ ) 0.425volts for Nd and 0.153volts for Li.

## Keywords:

Metallothermic; Molten Salt; Neodymium; E-pO<sup>2-</sup> diagram; STABCAL

## Dedication

I dedicate my thesis work to my family and many friends. I thank my brothers Danny; Dennie; Andri; my sister, Ketrin; my sister in law, Suzanna; and my girlfriend, Mellisa; for their support and pray as well.

I also dedicate this thesis to my friends who have encouraged me throughout the process. I deeply appreciate all their help and pray. I thank Gracia, Henri, Hansen, Henry, Afung, Yosafat, Albert, Wayan, Erlien, Imade, Stephen, Wenny, Mami Tjhia, Hadi, Henny, Rico, Roe, Niko, Jerry, Saori, and many others for all their support and help me throughout the process of getting master degree program.

Thanks to Leo, Feby, Didin, Fikri, Riri, Budi, Hery, Julian, Fransiska, Diana, Sandy, Anton, Kurnia, Melky, Abong, Olivia, Dendy and my other colleagues in Indonesia because they all also contribute to motivate me in finishing this thesis.

Lastly, a special thanks to Mom (Merry Sintawati) and Dad (Willie Gunawan) for all their tremendous love and support to motivate me in finishing this work; without them this work will unlikely to be done.

## Acknowledgements

I would like to thank my advisor and my committee, especially Dr. Hsin-Hsiung Huang, who persistently push, help, and guide me in completion of my thesis research. Remembering his enthusiastic to learn new things will always kindle my motivation to never stop learning.

I would also like to express my gratitude to my parents that always supporting me financially, and Dr. Courtney Young that gave me a scholarship and allow me to work as a teaching assistant. Without their assist, I would not have a tuition waiver and would have a huge amount of financial loan.

In addition, I would like to thank my other committee members, Professor Rod James and Jannette Chorney, who willingly become my committee member and will give me a positive feedback to refine my thesis work.

# Table of Contents

|  |      |
|--|------|
| ABSTRACT .....   | II   |
| DEDICATION .....   | III  |
| ACKNOWLEDGEMENTS .....   | IV   |
| TABLE OF CONTENTS.....   | V    |
| LIST OF TABLES .....   | VII  |
| LIST OF FIGURES.....   | VIII |
| 1. INTRODUCTION .....  | 1    |
| 1.1. Background .....  | 1    |
| 1.2. General Processes of Rare Earth .....   | 2    |
| 1.3. Major Rare Earth Ore deposit and Commercial Process .....   | 3    |
| 1.4. Reduction Process .....   | 6    |
| 2. RESEARCH OBJECTIVES.....  | 9    |
| 3. THERMODYNAMIC CONSIDERATIONS .....  | 10   |
| 3.1. Fused Salt .....  | 10   |
| 3.2. Molten Salt Electrolysis .....  | 16   |
| 3.3. Rare earth compounds' properties.....   | 19   |
| 3.4. Decomposition potential.....  | 21   |
| 3.5. Solubility.....   | 26   |
| 3.6. E-pO <sup>2-</sup> Diagram.....   | 30   |
| 4. IMPLEMENTING E-PO <sup>2-</sup> DIAGRAM FOR Nd <sub>2</sub> O <sub>3</sub> IN LiF-NdF <sub>3</sub> SYSTEM ..... | 41   |
| 4.1. Databases of HSC and Kubaschewski.....  | 42   |
| 4.2. Modeling E-pO <sup>2-</sup> diagram with STBCAL.....  | 43   |
| 5. RESULTS AND DISCUSSION .....  | 45   |
| 5.1. Reactions and potential Nd <sub>2</sub> O <sub>3</sub> in LiF-NdF <sub>3</sub> system.....                    | 45   |

|   |   |    |
|---|---|----|
| 5.2.  | <i>E-pO<sup>2</sup>- diagram of Nd<sub>2</sub>O<sub>3</sub> in LiF-NdF<sub>3</sub> system .....</i> | 46 |
| 5.3.  | <i>Decomposition Competition between Nd and Li Metals .....</i>                                     | 49 |
| 6.  | CONCLUSION .....  | 51 |
| REFERENCES CITED .....  |   | 53 |
| APPENDIX A: BINARY PHASE DIAGRAMS OF RARE EARTHS IN FLUORIDE SYSTEM (THOMA, 1965) ..... |   | 55 |

## List of Tables

|   |    |
|---|----|
| Table I. The abundance of rare earths and some common elements in the Earth's crust (EPA, 2012) .....                 | 2  |
| Table II. Melting point salt system (M.A. Bredig, 1963) .....   | 11 |
| Table III. Production of rare earth metal using molten salt electrolysis (Zhu, 2014).....                             | 19 |
| Table IV. Melting point (m.p) and boiling point (b.p) of rare earth metals and its compounds .....                    | 20 |
| Table V. Melting point (m.p.) and boiling point (b.p.) of rare earth metal subchloride, subfluoride .....             | 21 |
| Table VI. Results of electrolysis rare earth in laboratory scale using consumable anode (Osamu et al., 2014) .....    | 25 |
| Table VII. Results of electrolysis rare earth in industrial scale using consumable cathode (Osamu et al., 2014) ..... | 25 |
| Table VIII. Linear fitting parameters for data plots in Figure 11 (Guo, Sietsma, & Yang, 2014) .....                  | 27 |
| Table IX. Comparison of water and molten bath.....  | 33 |
| Table X. Selected condition in a fluoride system for modeling E-pO <sup>2-</sup> diagram .....                        | 41 |
| Table XI. Free energies formation of Nd in LiF <sub>3</sub> and NdF <sub>3</sub> at 1023.15°K .....                   | 43 |



## List of Figures

|  |    |
|--|----|
| Figure 1. General processes of extracting rare earth flow chart .....  | 3  |
| Figure 2. Major rare earth deposit and its reserve and production volume in oxide form...  | 4  |
| Figure 3. Simplified Yao Lung chemical plant's process flowsheet (Zhang et al., 1982) ....   | 5  |
| Figure 4. The binary phase diagram of KBr - KF system (Fact Sage, 2015) .....  | 11 |
| Figure 5. The binary diagram of KF-LaF <sub>3</sub> system (Thoma, 1965) .....   | 13 |
| Figure 6. Phase diagram of NaCl-CaCl <sub>2</sub> -NdCl <sub>3</sub> (Thoma, 1965) .....   | 13 |
| Figure 7. Imposed AC cell for electrowinning lanthanum (Morrice et al., 1962). .....   | 16 |
| Figure 8. Standard decomposition voltages of rare earth oxides at 1273°K (Osamu et al., 2014).<br>.....  | 22 |
| Figure 9. Standard decomposition voltage of rare earth chlorides and selected chloride salt<br>.....   | 23 |
| Figure 10. Standard decomposition voltage of rare earth fluorides and selected fluoride salt<br>.....  | 23 |
| Figure 11. Solubility of rare earth oxides in fluoride bath as a function of temperature...  | 26 |
| Figure 12. The solubility of rare earth oxides as a function of rare earth fluoride solvent content<br>.....   | 28 |
| Figure 13. Solubility of Ho, La, and Sm as a function of temperature in fluoride melts ..  | 29 |
| Figure 14. Solubility of Nd <sub>2</sub> O <sub>3</sub> solubility in LiF-Alkali Metal F <sub>2</sub> - NdF <sub>3</sub> (Guo, Sietsma, & Yang,<br>2014) ..... | 29 |
| Figure 15. Potential-pO <sup>2-</sup> diagram of Fe in NaNO <sub>3</sub> at 600°K .....  | 31 |
| Figure 16. Eh-pH diagram of Fe in water at 298°K .....   | 31 |

|  |    |
|--|----|
| Figure 17. E-pO <sup>2-</sup> diagram of La in molten NaCl:2CsCl molten bath at 600°C. The blue colored area showed the LaCl <sub>3</sub> dissolved and decomposed to La <sup>3+</sup> and Cl <sup>-</sup> .....   | 36 |
| Figure 18. E-pO <sup>2-</sup> diagram of La in the NaCl:2CsCl molten bath at 600°C. Stability of bath is shown by its decomposition potentials. The diagram also shows the potentials of anode and cathode reactions for extraction of La from the molten bath ..... | 38 |
| Figure 19. Binary diagram of NdF <sub>3</sub> with alkali metal fluoride (Grebnev and Dmitrienko, 2007) .....  | 42 |
| Figure 20. STABCAL's Interface .....   | 44 |
| Figure 21. E-pO <sup>2-</sup> diagram of Nd <sub>2</sub> O <sub>3</sub> in mole% 75LiF - mole%25 NdF <sub>3</sub> at 1023.15°K (HSC databases) .....   | 46 |
| Figure 22. E-pO <sup>2-</sup> diagram of Nd <sub>2</sub> O <sub>3</sub> in mole%75 LiF - mole%25 NdF <sub>3</sub> at 1023.15°K....   | 47 |
| Figure 23. Electrolysis of Nd in fluoride system illustration.....   | 49 |
| Figure 24. E-pO <sup>2-</sup> diagram of Nd <sub>2</sub> O <sub>3</sub> with additional formation of LiF potential. ....   | 50 |

# 1. Introduction

## 1.1. Background

Rare earth elements were discovered in the late 18th century, when the first recognized rare earth element, gadolinite was identified by the Finish chemist Johan Gadolin (C.K. Gupta & N. Krishnamurthy, 2005). Rare earths refer to 17 chemical elements in the periodic table that consists of lanthanides group (from lanthanum to lutetium), yttrium, and scandium. Rare earths share some common properties; such as: softness, ductility, malleability, reactivity and magnetic. Those properties, especially the latter and the fact rare earth magnets are the strongest type of magnets, make rare earths useful in many applications. Optical lenses, batteries, fiber optics, LCDs, and MRIs are some products that use rare earths as part of their composition.

Rare earths are considered rare not because they are in scarcity. All rare earths except promethium, are more abundant than gold which has 0.0031 ppm in the Earth's crust (Environmental Protection Agency [EPA], 2012). The abundance of rare earth and other common elements are depicted in Table I. The main reason why rare earths are called rare is due to the early difficulty in identifying them, because they exhibit similar chemical properties. Furthermore, they are typically found dispersed as rare earth oxides (REO) due to their affinity to oxygen, and are not often found in significant concentration. One example is lanthanum rare earth that is normally found as a combination of cerium with other rare earths, and oxidizes rapidly when exposed to air and hot water.

Lanthanum is the first lanthanide group of metallic element in Group 3 periodic table. Lanthanum is ductile, malleable, very reactive, and one of the richest rare earths on earth with 30 ppm crystal abundance (EPA, 2012). This silvery white, metallic rare earth element is widely used as fluid catalytic cracking, hydrogen batteries, camera, and telescope lenses.

**Table I. The abundance of rare earths and some common elements in the Earth's crust (EPA, 2012)**

| Elements  | Crustal Abundance<br>(parts per million) |
|---|--|
| Nickel ( $_{28}\text{Ni}$ )                             | 90                                       |
| Zinc ( $_{30}\text{Zn}$ )                               | 79                                       |
| Copper ( $_{29}\text{Cu}$ )                             | 68                                       |
| <b>Cerium (<math>_{58}\text{Ce}</math>)<sup>a</sup></b> | <b>60.0</b>                              |
| <b>Lanthanum (<math>_{57}\text{La}</math>)</b>          | <b>30.0</b>                              |
| Cobalt ( $_{27}\text{Co}$ )                             | 30                                       |
| <b>Neodymium (<math>_{60}\text{Nd}</math>)</b>          | <b>27.0</b>                              |
| <b>Yttrium (<math>_{39}\text{Y}</math>)</b>             | <b>24.0</b>                              |
| <b>Scandium (<math>_{21}\text{Sc}</math>)</b>           | <b>16.0</b>                              |
| Lead ( $_{82}\text{Pb}$ )                               | 10                                       |
| <b>Praseodymium (<math>_{59}\text{Pr}</math>)</b>       | <b>6.7</b>                               |
| Thorium ( $_{90}\text{Th}$ )                            | 6  |
| <b>Samarium (<math>_{62}\text{Sm}</math>)</b>           | <b>5.3</b>                               |
| <b>Gadolinium (<math>_{64}\text{Gd}</math>)</b>         | <b>4.0</b>                               |
| <b>Dysprosium (<math>_{66}\text{Dy}</math>)</b>         | <b>3.8</b>                               |
| Tin ( $_{50}\text{Tn}$ )                                | 2.2                                      |
| <b>Erbium (<math>_{68}\text{Er}</math>)</b>             | <b>2.1</b>                               |
| <b>Ytterbium (<math>_{70}\text{Yb}</math>)</b>          | <b>2.0</b>                               |
| <b>Europium (<math>_{63}\text{Eu}</math>)</b>           | <b>1.3</b>                               |
| <b>Holmium (<math>_{67}\text{Ho}</math>)</b>            | <b>0.8</b>                               |
| <b>Terbium (<math>_{65}\text{Tb}</math>)</b>            | <b>0.7</b>                               |
| <b>Lutetium (<math>_{71}\text{Lu}</math>)</b>           | <b>0.4</b>                               |
| <b>Thulium (<math>_{69}\text{Tm}</math>)</b>            | <b>0.3</b>                               |
| Silver ( $_{47}\text{Ag}$ )                             | 0.08                                     |
| Gold ( $_{79}\text{Au}$ )                               | 0.0031                                   |
| Promethium ( $_{61}\text{Pm}$ )                         | $10^{-18}$                               |

## 1.2. General Processes of Rare Earth

Rare earths generally can be extracted in five general steps. It starts with the mining processes where rare earths are mined via either surface or underground mining. Mining process is followed by the beneficiation process-by crushing, grinding, flotation, thickening and drying. The next step is to separate rare earths from their impurities. Solvent extraction, washing, filtering and drying/calcining are generally used in these separation processes. The fourth step is the reduction process to produce rare earths. Results of this process are rare earth metals with 98-99% purity. The last step is the refining process to produce lanthanum with at least 99.5% purity. The fourth and fifth processes can be optional depending on the market demands. These processes can be simplified with a flowchart in Figure 1.

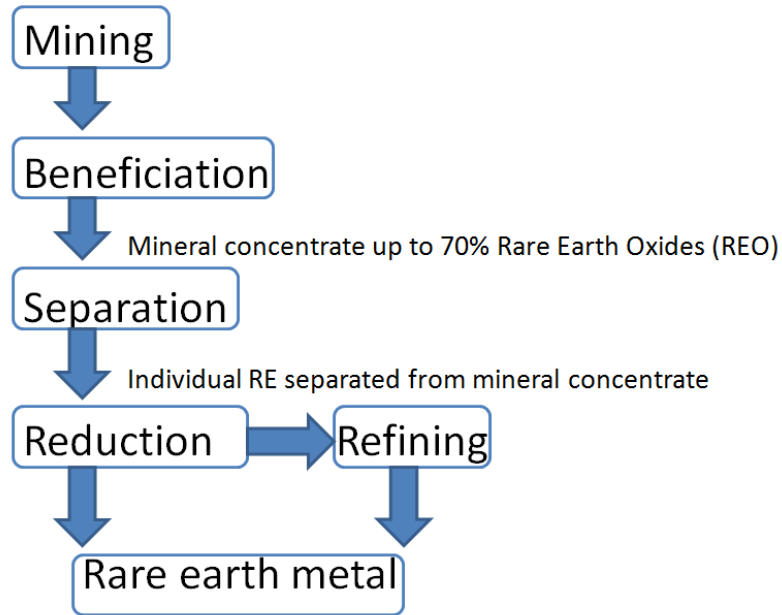


**Figure 1. General processes of extracting rare earth flow chart**

### **1.3. Major Rare Earth Ore deposit and Commercial Process**

The major mineral resources of rare earth can be found in bastnasite ( $\text{Ln}(\text{CO}_3)\text{F}$ ), xenotime ( $\text{YPO}_4$ ), and monazite ( $\text{LnPO}_4$ ), where Ln is referred to lanthanides (Gupta & Krishnamurthy, 2005). These three type of minerals contribute up to 95% rare earth resources in the world. Each of those minerals exhibit dissimilar characteristics and properties that subsequently should be treated in a different manner. Figure 2 depicts major ore deposits, their reserves, and production volume in the world in 2010 (Osamu & Toru, 2014).

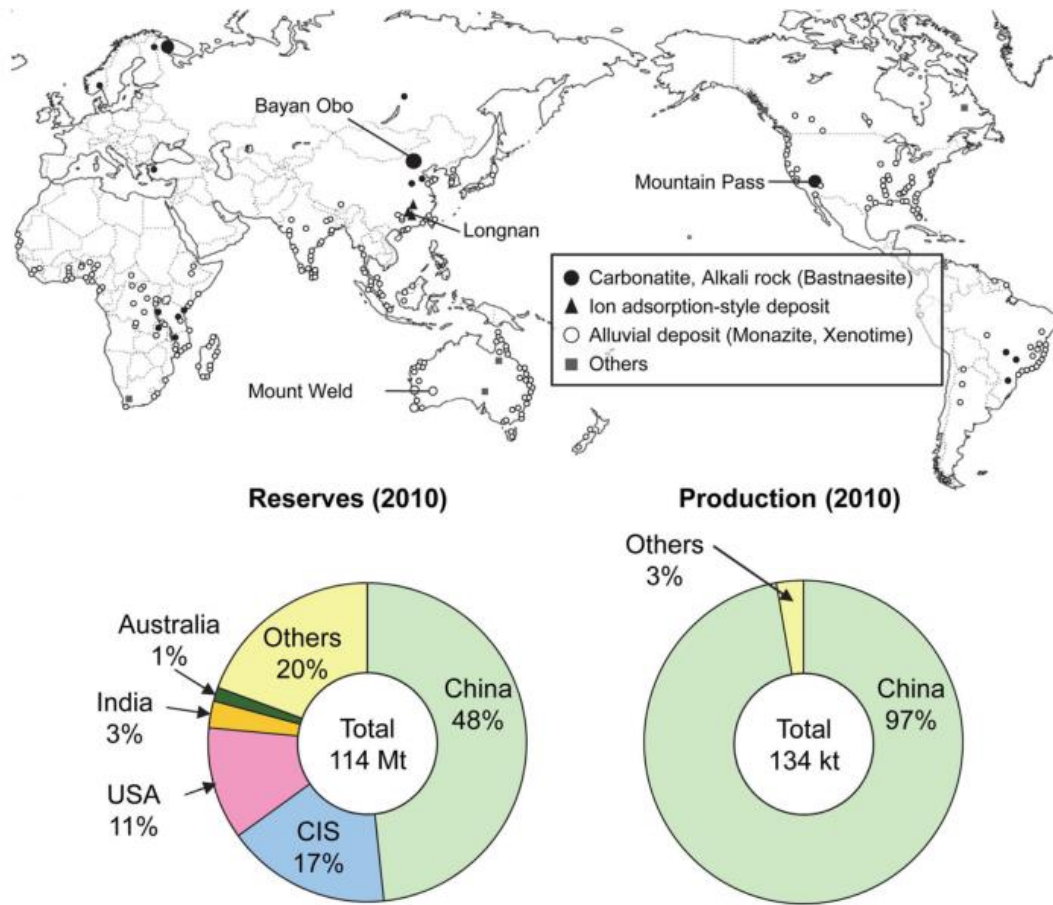


**Figure 2. Major rare earth deposit and its reserve and production volume in oxide form (Osamu & Toru 2014)**

Figure 2 shows the major ores of rare earths (bastnaesite, xenotime, and monazite) that are spread all over the world with an abundant amount of reserves, where China still dominates the rare earth production in oxide form.

One example of a rare earth processing plant in China is depicted in Figure 3 at Yao Lung chemical plant that processes monazite mineral into RE metal, Rare Earth Oxide (REO), and RE alloy (Zhang et al., 1982).

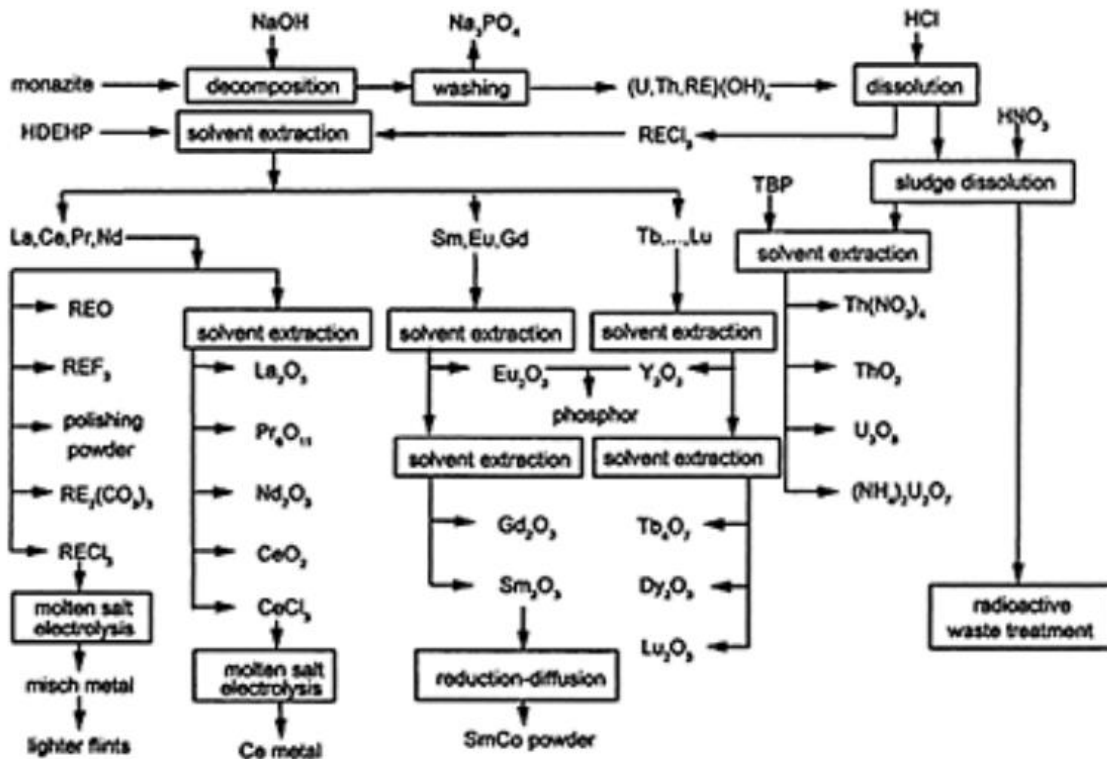


Figure 3. Simplified Yao Lung chemical plant's process flowsheet (Zhang et al., 1982)

Figure 3 shows the first rare earth processing plant in China; which started production commercially in 1964. The Yao Lung plant produces variety of rare earths products such as REO, REF, RECl<sub>3</sub>, Ce metal and misch-metal (combination of rare earth metals) using solvent extraction, electrolysis and reduction processes.

The flowsheet illustrates that most of RE are extracted to REO, with only cerium pure metal reduced from cerium compound by molten salt electrolysis. This is occurred due to the characteristic of REO such as: high stability and low solubility, that makes reduction process hard to be done. Nevertheless, research and experimentation on the extraction of rare earths is still being conducted to find an effective method to extract and separate rare earths. And now, more rare earth metals can be extracted such as: Nd, Dy, Gd, Pr, and Sc by the metallurgical or electrolysis reduction process.

## 1.4. Reduction Process

As rare earth oxide compounds are very stable, the reduction process is really difficult. Many ways to reduce rare earth oxides to become rare earth metals or alloys have been experimented, and they can be categorized mainly into two methods. The first is a metallothermic, a reduction process that is determined by free energy of formation of the compounds, melting point, boiling point, vapor pressure, density, reducing agents, and viscosity. Another method is an electrolytic process that relates not only to chemical stability, but also decomposition potential (Gupta & Krishnamurthy, 2005).

### 1.4.1. Metallothermic

Converting rare earth oxide into rare earth chloride or fluoride, and then converting those rare earth halides into rare earth metal are the general processes in metallothermic reduction. Rare earth oxides normally have standard free energy of formations higher than most compounds, which make them really stable. Based on the standard free energy value, only a few compounds such as calcium oxide and halide that generally have a higher free energy of formation than the most of rare earth oxides and halides respectively. Hence, rare earths will react with those reducing agents that are more stable.

Metallothermic process can be done in some ways depending on what type of rare earths. One of the ways is a lithium reduction using distillation for rare earth chlorides such as: Dy, Ce, and Er; that is conducted in two steps. The first step is distilling lithium vapor into liquid rare earth chloride. The second step is distilling lithium chloride slag (as it reacted with rare earth chloride) and an excess of reducing agent. This operation is carried out at 900°C using pure lithium or lithium with 5% calcium as a reducing agent (Gupta & Krishnamurthy, 2005).



That method requires intermediate processes before entering the reduction step such as: hydrating rare earth to rare earth chlorides or fluorides, dehydrating rare earth halides, and purification of those rare earth halides. These preparation processes are also applied to other metallothermic processes.

The purity of rare earth products using metallothermic processes depends on these preparation processes and reducing agents. Hence, the preparation processes are very critical in determining the quality of rare earth products.

#### **1.4.2. Electrolytic Reduction**

Electrolytic process is the most common method for extracting Ce, La, Nd, Dy, Pr, Gd, Y, Sc, and misch metal rare earths. As mentioned before, this process considers decomposition potential, therefore a particular voltage (above decomposition potential) is applied in the electrolyte cell to make rare earth compounds decompose and deposit as rare earth metal at the cathode, which normally consist of W or Mo metal (Osamu, Tetsuya & Toru, 2014).

Unlike metallothermic, the electrolysis process can run continuously in a high volume of production. Furthermore, this process is relatively less elaborate than metallothermic, especially in the preparation processes. This method has also shown a promising outcome that results in ongoing electrolysis development process to lead a better effectiveness and efficiency. It is also reflected by the most popular misch-metal produced from electrolysis reduction process, and INFINIUM inc.; which headquartered in Boston, U.S., has developed their electrolytic process technology and started to enter commercial production to produce rare earth products such as: dysprosium-iron (Dy-Fe) and neodymium metal in 2014.

As stated earlier, the electrolytic process shows promising results for some rare earths and has been used to produce the largest quantity of rare earth metals (Gupta & Krishnamurthy,

2005). This process requires a high temperature condition for which an aqueous solution is not suitable to be used as an electrolyte medium. Hence, a molten salt is selected as the carrier that can withstand with a high temperature condition. With this condition, a rare earth that has high melting temperature will be dissolved in a molten salt and will be collected in the cathode of the cell eventually.

Unlike aqueous solutions, molten salts can behave differently as the temperature changes, therefore a thermodynamic study on molten salt electrolyte at elevated temperature is essential to achieve effectiveness electrolysis process of rare earths. Moreover, understanding important considerations of the electrolytic process will enable to make the best use of the electrolytic process.

This work will describe the importance of thermodynamic considerations in the electrolytic process, and present the thermodynamic data in a  $E-pO^{2-}$  diagram, which is a diagram of equilibrium potential ( $E$ ) in a selected system that plotted against the activity of oxide ( $O^{2-}$ ) in the molten melt that was introduced by Littlewood (1962). This diagram has a similar function with a Pourbaix diagram that is convenient to outline the thermodynamic properties in a system, except  $E-pO^{2-}$  diagram can be utilized in a fused salt system that operates at elevated temperature.

## 2. Research Objectives

There were two main objectives in this research. The first objective was to conduct an analysis of the electrolytic process of rare earths based on its thermodynamic considerations. The other objective was to implement E-pO<sup>2-</sup> diagram in the electrolysis of rare earth to provide a fundamental information to obtain an effective electrolytic process. For the second objective, this study was limited to the electrolysis process with rare earth oxide as the feed in a fluoride fused salt system.

The important considerations that would be analyzed were: electrolysis process, fused salts, properties of rare earth oxides in a fused salt system, decomposition potential, solubility, and the use of E-pO<sup>2-</sup> diagram. The solubility was limited to molten fluorides system. Various researchers have previously performed a number of studies that were used as sources to support electrolytic process evaluations.

Lastly, E-pO<sup>2-</sup> diagram was modeled and implemented for one example in the electrolysis of a rare earth, to give an essential thermodynamic information plotted in a single graph. This work will select a neodymium oxide in fluorides melt with composition of LiF - 75mole% and NdF<sub>3</sub> – 25mole% at 750°C.

This system was chosen and limited to a fused salt that consisted of a mixture of two compounds. E-pO<sup>2-</sup> diagram was modeled and constructed using STABCAL; a program that calculates, simulates and models chemical equilibrium in either aqueous or non-aqueous systems, to construct and outline E-pO<sup>2-</sup> diagram in a selected fused salt system.

### **3. Thermodynamic Considerations**

#### **3.1. Fused Salt**

Fused salt or molten salt is a salt that is solid at ambient temperature and enters the liquid phase at elevated temperature. A molten salt has a low viscosity, high heat capacity, and high electric and thermal conductivity. This electrolyte has been used for some applications like transferring heat in solar tower, as a catalyst in coal gasification, in a molten salt reactor. It can also be used for extracting non-ferrous metals such as: aluminum, titanium, magnesium (in chloride bath) and rare earths by electrolysis. Comparing with the molten salts' properties, the aqueous solutions have some limitations in some application such as: cannot withstand at a high temperature condition; cannot transfer heat sufficiently; have a higher energy of formation (less reactive) than rare earth oxides, which make the reaction unlikely to occur in extracting rare earth oxides (Brajendra & David, 2004).

On the downside, fused salts are corrosive especially when an oxidant is present, and have a volume expansion upon melting of about 25%. These properties can cause adverse effect in some application and severely damage the environment. Nevertheless, the ongoing research of the thermodynamics, chemistry, and electrochemistry of fused salt is still needed so the fused salt technology can fully be understood and developed in the future.

##### **3.1.1. Fused Salts Mixture**

Fused salts are in a solid state at room temperature, therefore, it requires heat to raise the temperature above its melting point to ensure the fused salt remains in the molten state as an electrolyte in the electrolysis process. The melting point of several fused salts are shown in Table II.

**Table II. Melting point salt system (M.A. Bredig, 1963)**

| Melting point (°C)    | F <sup>-</sup> | Cl <sup>-</sup> | Br <sup>-</sup> | I <sup>-</sup> |
|-----------------------|----------------|-----------------|-----------------|----------------|
| <b>Li<sup>+</sup></b> | 848            | 610             | 550             | 469            |
| <b>Na<sup>+</sup></b> | 995            | 800             | 747             | 660            |
| <b>K<sup>+</sup></b>  | 857            | 770             | 734             | 681            |
| <b>Rb<sup>+</sup></b> | 795            | 722             | 692             | 647            |
| <b>Cs<sup>+</sup></b> | 703            | 645             | 636             | 626            |

Table II depicts that iodine salt system has the lowest melting point temperature compared to other halide salts ( $I < Br < Cl < F$ ). Fused salts have a high melting temperature that requires high energy consumption. In other words, electrolysis of rare earths is a high cost process. One of the most efficient ways to reduce cost, which is the desire of every industry, is by reducing the energy consumption. A mixture of fused salts generally possesses a lower melting point than a single fused salt system, therefore, a lower heat will be needed to maintain a molten fused salt, which leads to cost efficiency. Figure 4 shows a phase diagram for a mixture of two molten salts that presents a lower melting point.

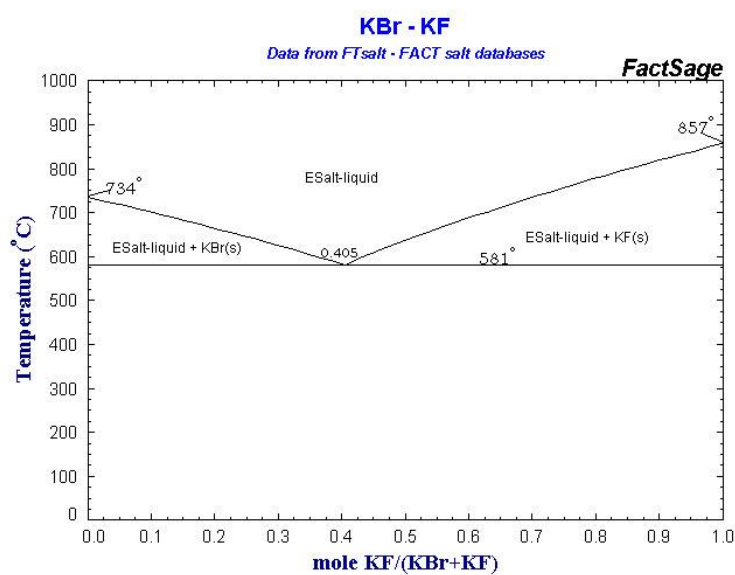
**Figure 4. The binary phase diagram of KBr - KF system (Fact Sage, 2015)**

Figure 4 shows the binary phase diagram of KBr, which has a 734°C melting point; and KF, which has 857°C melting point. By mixing it together, this fused salt mixture can attain a liquid state at 581°C, which is 153°C lower than the melting point of KF itself. The lowest melting point of this system occurs at the eutectic point at 40.5% of KF mole. This can be applied to other combinations of fused salts or even rare earth compounds as well. Subsequently, rare earth metal production by molten salt electrolysis have been using a fused salt mixture as the electrolyte in an attempt to save on their costs by having a lower operating temperature instead of using one fused salt system. Furthermore, a few types of molten salts, such as alkali metal fluoride and rare earth fluoride salts can also help to increase the solubility of the rare earth oxide as the feed material, which will be explained in further details in Chapter 3.5.

An important thing to consider in selecting a combination of fused salts, is the formation of complex compounds or solid compounds in electrolysis process. In some cases, a complex compound or solid compound can be formed that makes the electrolysis process become more difficult for rare earth extraction. For instance, a binary system of KF-LaF<sub>3</sub>, which is illustrated in Figure 5, has a melting point of 620°C at its eutectic point with 22 mole % of LaF<sub>3</sub>. If the mole % composition is changed slightly to < 22 mole %, KF solid will be formed at 620°C, which is undesirable because that fused salt is becoming solidified. On the other hand, if the mole % of KF increase above >22 mole % at 620°C, KF.LaF<sub>3</sub> solid will be formed, and consequently, the lanthanum rare earth will not decompose as lanthanum metal in the cathode. Some other binary phase diagrams of rare earths in fluoride systems are illustrated in Appendix A.

A three component system has also been used in the molten salt and its eutectic point can be found in the three component phase diagram that is shown in Figure 6.

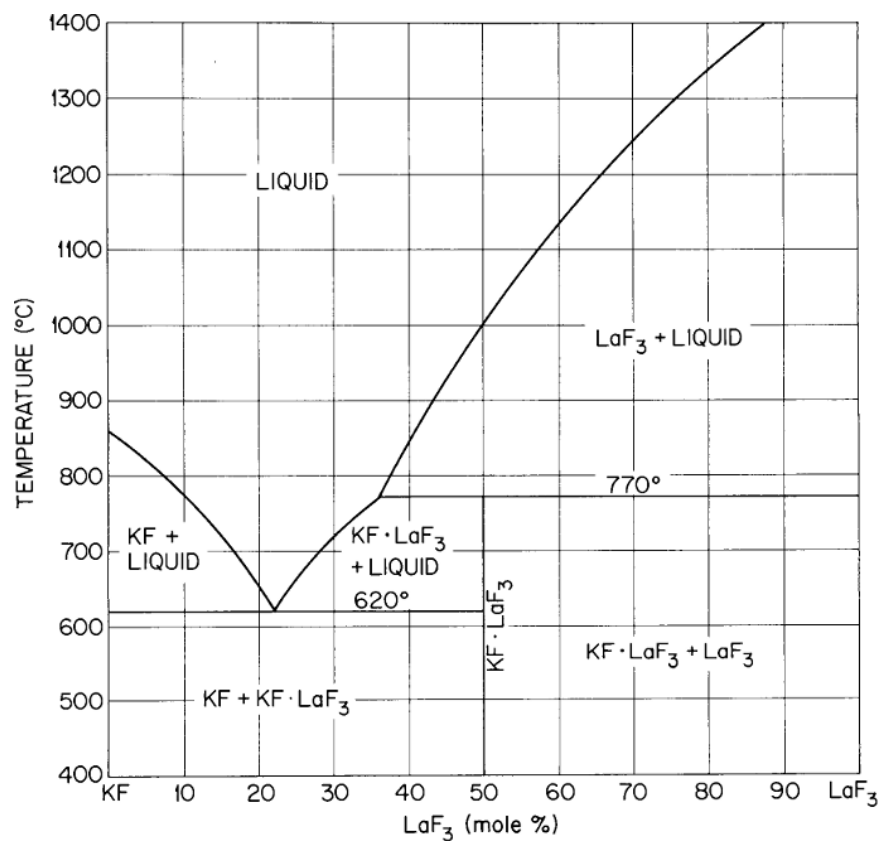


Figure 5. The binary diagram of KF-LaF<sub>3</sub> system (Thoma, 1965)

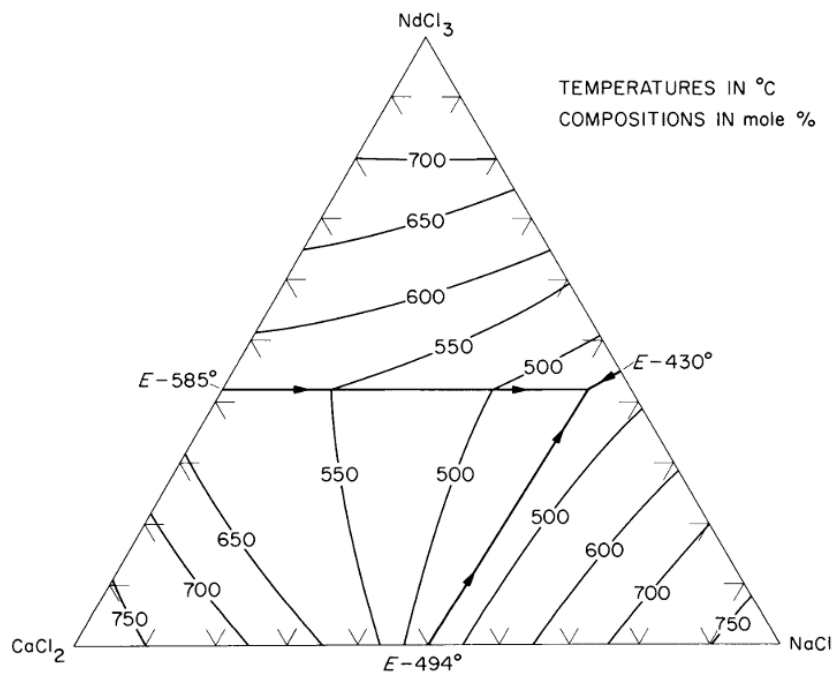


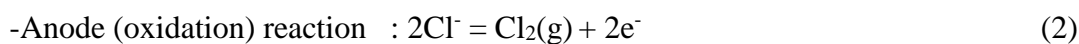
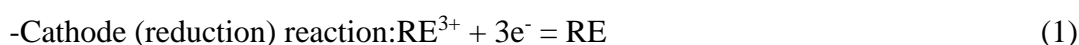
Figure 6. Phase diagram of NaCl-CaCl<sub>2</sub>-NdCl<sub>3</sub> (Thoma, 1965)

Figure 6 is a ternary phase diagram of the NaCl-CaCl<sub>2</sub>-NdCl<sub>3</sub> system illustration of that produces a lower melting point rather than melting point for each compound. Neodymium chloride (NdCl<sub>3</sub>) is added as a component of a chloride mixture not only to lower the melting point, but also to help dissolving process instead of using rare earth oxide as the sole feed.

There has been a lack of research on bromides and iodides; therefore there is inadequate thermodynamic information about oxidation state or crystal chemistry of them with other halides, so they are still infeasible to be used as electrolytes in the electrolysis of rare earths (Thoma, 1965). Subsequently, there are only two type of fused salts that are commonly used in the electrolysis of rare earth metals: chloride and fluoride salts.

### 3.1.2. Molten Chloride Salt

Electrolysis of rare earth chlorides has been investigated since the early twentieth century and it has been utilized to produce La, Ce, Pr, Nd, and misch-metal. Before 1997, China which is the biggest rare earth producer, mostly used the chloride system for electrolysis of rare earths until they substituted fluoride-oxide system for it (Zhu, 2014). The general reactions that present in chloride system are:



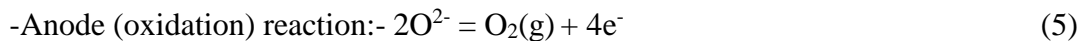
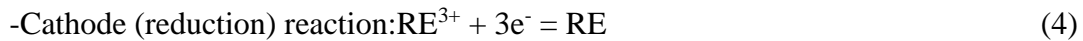
The chloride salt system is appropriate for misch-metal and rare earth metals that have a low melting point. The raw materials for producing the misch-metal rare earth in electrolysis are rare earth chlorides. Before feeding into the chloride molten bath, this raw material is dehydrated at around 400°C, because it can reduce the current efficiency during the electrolysis. While the chloride system is employed due to the lower cost compared to the fluoride system, it is



unseemly to be used at high temperature operating conditions due to a lower melting point compared to the fluoride system, high hygroscopicity, and high volatility. At high temperature, solubility of metals in the chloride bath will increase drastically and damage the cell wall of the electrolysis process. Furthermore, the current efficiency in the chloride system is lower than fluoride system (Zhu, 2014).

### 3.1.3. Molten Fluoride Salt

Unlike the chloride system, the fluoride system has a higher melting point which enables it to perform at higher temperature conditions, thus it is appropriate for processing rare earths with higher melting temperatures, such as terbium, dysprosium, or gadolinium. Initially, this system was utilized to produce misch-metal rare earths in the 1970s in Japan, then it was becoming largely produced due to an increasing demand of Nd alloys (Osamu Takeda et al., 2014). The reactions that occur in this system are:



This system utilizes rare earth oxide or fluoride compounds as the feed, while the chloride system normally uses rare earth chloride or fluoride compounds. The oxides as raw feed is needed to prevent oxidation of fluorine in the anode which hinders the electrolysis process. However, overfeeding of oxides can form a sedimentation of insoluble compounds in the cell as impurities. Unlike rare earth chlorides, rare earth fluorides are stable and not hygroscopic, that leads to easier control of purity in the electrolyte. It also has more current efficiency than chloride system, yet is compromised by the high energy consumption around 10.6kWh/kg (Zhu,

2014). Moreover, corrosion and low solubility of oxides in the fluoride bath seem to be the main issues in this process.

### 3.2. Molten Salt Electrolysis

Molten salt electrolysis process occurs when two electrodes (an anode and a cathode) are immersed in the molten salt with a particular voltage that will reduce the rare earth compound and deposit it at the cathode. This process uses molten salt or fused salt as the electrolyte carrier because it has an excellent heat capacity and can attain temperatures up to 1000°C, while electrolysis using aqueous solution is implausible due to the high stability that rare earths have.

Molten salt electrolysis has been replacing metallothermic processes to produce some rare earths because this method is continuous, relatively simple and economical (Stefanidaki, Hasiotis, & Kontoyannis, 2001). Figure 7 shows an example of electrolysis for lanthanum.

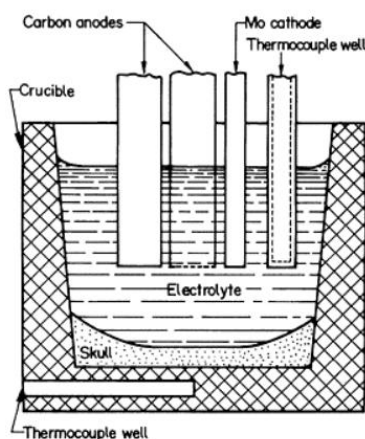


**Figure 7. Imposed AC cell for electrowinning lanthanum (Morrice et al., 1962).**

Figure 7 depicts an electrowinning process of lanthanum oxide in  $\text{LaF}_3\text{-LiF-BaF}_2$  bath experimented by Morrice et al. (1962). Alternating current (AC) was connected on the two graphite anodes, and was used to heat and maintain the electrolyte temperature during the operation, while direct current (DC) power was connected to the carbon anodes and molybdenum

cathodes. The skull or a frozen bath was formed during this electrolysis process, and served to prevent rare earth contact with the crucible.

Anode, cathode and electrolyte are three main components that make this process attainable. At the anode, the oxidation reaction occurs; while at the cathode, the reduction reaction occurs with molten salt as the carrier electrolyte. The anode is normally made from graphite, due to the oxidation process it is easier instead of using inert material. Furthermore, this consumable graphite in the anode will react with oxygen in the anode (oxidation process) then creates an exothermic reaction which produces heat to help maintain the operation temperature process. As for the cathode, is generally made from molybdenum or tungsten, which are non-consumable cathodes and do not react with the deposition of the rare earth. Iron can also be utilized as a cathode, which is consumable and forms a rare earth alloy (RE-Fe) as the final product.

### **3.2.1. Current Efficiency**

#### **3.2.1.1. Current Efficiency Chloride Electrolysis**

In chloride electrolysis, the current efficiency is generally below 50% in industry, which is quite low compare to fluoride electrolysis (Zhu, 2014). The current efficiency in the electrolysis process can be affected by some factors such as: temperature, current density, impurities, and feed materials. One particular reason for this low current efficiency is the existence of divalent ions ( $\text{RE}^{2+}$ ) during electrolysis process. This phenomena occurs to all rare earths that will form highly stable divalent ions in the chloride electrolysis. Thereafter, the reactions in the cathode will be undergone in two steps, while in the anode,  $\text{RE}^{2+}$  can be oxidized back to  $\text{RE}^{3+}$ . In some cases, tetravalent oxidation states at the chloride melts can also be present, and be quite unstable. The forming reactions of  $\text{RE}^{2+}$  in the electrodes are:



Reaction 7 and 9 shows a cyclic reactions of  $\text{RE}^{3+}/\text{RE}^{2+}$  and  $\text{RE}^{2+}/\text{RE}^{3+}$  respectively, which makes rare earths difficult to deposit at the cathode, and result in a low current efficiency.

Another cause for the low current efficiency is the presence of water in the electrolysis process. Rare earths have an affinity with water, and without proper treatment, rare earths' feed will contain water from their surrounding environment. Ultimately, it will decrease the current efficiency in the rare earth electrolysis process.

### **3.2.1.2. Current Efficiency Fluoride Electrolysis**

Fluoride electrolysis generally has a higher current efficiency compared to chloride electrolysis. It is reported that the current efficiency is generally above 65% (Zhu, 2014), because divalent ions are unlikely to be present in this electrolysis for most rare earths (relatively not stable in fluorides melts). Some industrial metal production of molten salt electrolysis chlorides and fluorides can be seen in Table III.

**Table III. Production of rare earth metal using molten salt electrolysis (Zhu, 2014)**

| Rare earth metals                     | Chloride electrolyte   | Current efficiency (%) | Fluoride electrolyte  | Current efficiency (%) |
|---------------------------------------|------------------------|------------------------|---|------------------------|
| <b>La</b>                             | LaCl <sub>3</sub> -KCl | 30-50                  | LaF <sub>3</sub> -LiF-La <sub>2</sub> O <sub>3</sub>                | Max 87                 |
| <b>Ce</b>                             | CeCl <sub>3</sub> -KCl | 30-50                  | CeF <sub>3</sub> -LiF-Ce <sub>2</sub> O <sub>3</sub>                | Max 87                 |
| <b>Gd</b>                             | -                      | -                      | GdF <sub>3</sub> -LiF-Ga <sub>2</sub> O <sub>3</sub><br>Gd-Fe alloy | Up to 82               |
| <b>Pr</b>                             | PrCl <sub>3</sub> -KCl | 35-40                  | PrF <sub>3</sub> -LiF-Pr <sub>2</sub> O <sub>3</sub>                | Up to 82               |
| <b>Dy</b>                             | -                      | -                      | Dy-Fe alloy   | Up to 80               |
| <b>Nd</b>                             | -                      | -                      | NdF <sub>3</sub> -LiF-Nd <sub>2</sub> O <sub>3</sub>                | ~80                    |
| <b>Yb</b>                             | -                      | -                      | YbF <sub>3</sub> -LiF-Yb <sub>2</sub> O <sub>3</sub>                | ~80                    |
| <b>Mixed rare earth (misch metal)</b> | ReCl <sub>3</sub> -KCl | 35-50                  | Re <sub>2</sub> O <sub>3</sub> -REF-LiF                             | ~65                    |

Table III shows that fluoride electrolyte has a higher efficiency than chloride electrolyte, and has been used to produce more types of rare earths. Table III also shows a mixture of molten salt using rare earth compound itself to reduce its melting point. Different current efficiency of cerium metal in fluorides system was stated by Osamu et al., (2014), which expressed that the current efficiency was 22%. This occurred due to the presence of a stable tetravalent ions of Ce in the fluoride system that lowered the current efficiency. Tetravalent ions of terbium were also found to be present in the fluoride bath (Boghosian, 1996).

### 3.3. Rare earth compounds' properties

In the chloride bath, the feed materials mostly are as rare earth fluoride and chloride compounds. As for fluoride bath, rare earth oxide and fluoride are the predominant feed materials. Rare earth chloride as the feed requires extra care to prepare it, because it is hygroscopic and presence of water can reduce the current efficiency. In the other hand, rare earth

fluoride is not hygroscopic, therefore it makes it easier to control the purity of the electrolyte resulting in a higher efficiency (Osamu et al., 2014).

Melting and boiling points for rare earth metals and compounds can be seen in Table IV. As an atomic number increases (lanthanum to lutetium), melting points of rare earth metals and rare earth oxides do not show an increasing or a decreasing tendency (fluctuating). Nevertheless, rare earth oxides exhibit an enormous melting and boiling points, which is one of the reasons why extracting rare earth oxides is extremely difficult.

**Table IV. Melting point (m.p) and boiling point (b.p) of rare earth metals and its compounds (Osamu et al., 2014)**

| Element<br>Ln | Metal, Ln                    |                              | Oxide, Ln <sub>2</sub> O <sub>3</sub> |                              | Fluoride, LnF <sub>3</sub>   |                              | Chloride, LnCl <sub>3</sub>  |                              |
|---------------|------------------------------|------------------------------|---------------------------------------|------------------------------|------------------------------|------------------------------|------------------------------|------------------------------|
|               | m.p., T <sub>m</sub><br>(°C) | b.p., T <sub>b</sub><br>(°C) | m.p., T <sub>m</sub><br>(°C)          | b.p., T <sub>b</sub><br>(°C) | m.p., T <sub>m</sub><br>(°C) | b.p., T <sub>b</sub><br>(°C) | m.p., T <sub>m</sub><br>(°C) | b.p., T <sub>b</sub><br>(°C) |
| <b>Sc</b>     | 1539                         | 2828                         | 2489                                  | -                            | 1552                         | 1879                         | 957                          | 967                          |
| <b>Y</b>      | 1526                         | 3334                         | -                                     | -                            | 1162                         | 2635                         | 709                          | 1501                         |
| <b>La</b>     | 920                          | 353                          | 2256                                  | 3620                         | 1500                         | 2359                         | 862                          | 1729                         |
| <b>Ce</b>     | 798                          | 3422                         | 2210                                  | 3730                         | 1436                         | 2161                         | 817                          | 1674                         |
| <b>Pr</b>     | 931                          | 3507                         | 2183                                  | 3760                         | 1401                         | 2222                         | 786                          | 1645                         |
| <b>Nd</b>     | 1016                         | 3064                         | 2233                                  | 3760                         | 1378                         | 2283                         | 759                          | 1648                         |
| <b>Pm</b>     | -                            | -                            | 2320                                  | -                            | 1344                         | 2330                         | 737                          | 1628                         |
| <b>Sm</b>     | 1072                         | 1788                         | 2269                                  | 3780                         | 1309                         | 2397                         | 681                          | -                            |
| <b>Eu</b>     | 817                          | 1525                         | 2291                                  | 3790                         | 1258                         | 2682                         | 624                          | -                            |
| <b>Gd</b>     | 1312                         | 3262                         | 2339                                  | 3900                         | 1235                         | 2427                         | 602                          | 1576                         |
| <b>Tb</b>     | 1357                         | 3219                         | 2303                                  | -                            | 1182                         | 2546                         | 582                          | 1554                         |
| <b>Dy</b>     | 1409                         | 2558                         | 2228                                  | 3900                         | 1160                         | 2571                         | 648                          | 1536                         |
| <b>Ho</b>     | 1470                         | 2691                         | 2330                                  | 3900                         | 1147                         | 2255                         | 708                          | 1514                         |
| <b>Er</b>     | 1522                         | 2859                         | 2344                                  | 3920                         | 1147                         | 2532                         | 774                          | 1508                         |
| <b>Tm</b>     | 1545                         | 1944                         | 2341                                  | 3945                         | 1158                         | 2294                         | 824                          | 1486                         |
| <b>Yb</b>     | 824                          | 1192                         | 2355                                  | 4070                         | 1172                         | 2427                         | 860                          | -                            |
| <b>Lu</b>     | 1663                         | 3391                         | 2427                                  | 3980                         | 1180                         | 2309                         | 904                          | 1456                         |

A decreasing melting point trend is found in rare earth fluorides, while it does not happen for the boiling point. In rare earth chlorides, a decreasing trend is found at their boiling point as the atomic number increases.

Melting points of few selected rare earths' divalent ions are presented in Table V, since divalent ions can occur especially in the chloride bath.

**Table V. Melting point (m.p.) and boiling point (b.p.) of rare earth metal subchloride, subfluoride (Boghossian et al., 1996)**

| Rare earth | LnCl <sub>2</sub> (Chloride) |                           | LnF <sub>2</sub> (Fluoride) |                           | LnF <sub>3</sub> (Fluoride) |                           |
|------------|------------------------------|---------------------------|-----------------------------|---------------------------|-----------------------------|---------------------------|
|            | m.p., T <sub>m</sub> (°C)    | b.p., T <sub>b</sub> (°C) | m.p., T <sub>m</sub> (°C)   | b.p., T <sub>b</sub> (°C) | m.p., T <sub>m</sub> (°C)   | b.p., T <sub>b</sub> (°C) |
| <b>Sc</b>  | 805                          | -                         | -                           | -                         | -                           | -                         |
| <b>Ce</b>  | -                            | -                         | -                           | -                         | 400                         | -                         |
| <b>Nd</b>  | 841                          | -                         | -                           | -                         | -                           | -                         |
| <b>Sm</b>  | 858                          | 1950                      | 1417                        | -                         | -                           | -                         |
| <b>Eu</b>  | 744                          | 2190                      | 1416                        | -                         | -                           | -                         |
| <b>Tb</b>  | -                            | -                         | -                           | -                         | 180                         | -                         |
| <b>Dy</b>  | 721                          | -                         | -                           | -                         | -                           | -                         |
| <b>Tm</b>  | 718                          | -                         | -                           | -                         | -                           | -                         |

Table V shows that divalent ions of Sm and Eu can also occur in the fluoride bath, while Sc, Nd, Sm, Eu, Dy, and Tm are present in the chloride bath. As mentioned earlier, rare earths can form a state of divalent ions, subsequently there will be a cyclic redox reaction in the electrolysis. Hence, some of these elements are not processed in industrial electrolysis scale.

### 3.4. Decomposition potential

Decomposition potential can be defined as a particular voltage required for the electrolysis process to occur. It is essential to understand the value so the desired compound (in this case rare earth) can decompose in the electrolytic cell and then deposit in the cathode. Decomposition potential can be found from standard Gibbs free energy formation ( $\Delta G$ ). This free energy change shows the tendency of a process to take place or not under particular temperature and pressure. The free energy formation can be expressed by equation:

$$\Delta G = - n. F. E \quad (10)$$

Where n, F, E are number of electrons, Faraday constant (23060 cal/volt.equivalent), and potential (volt) respectively. A spontaneous reaction is expressed as a negative value of  $\Delta G$ .

Decomposition potential of REO at 1273°K is depicted at Figure 8. It includes decomposition voltage of CaO as a reference and shows an increasing tendency as atomic number increases. It also shows that Eu has the lowest decomposition voltage, while the highest are Sc and Y.

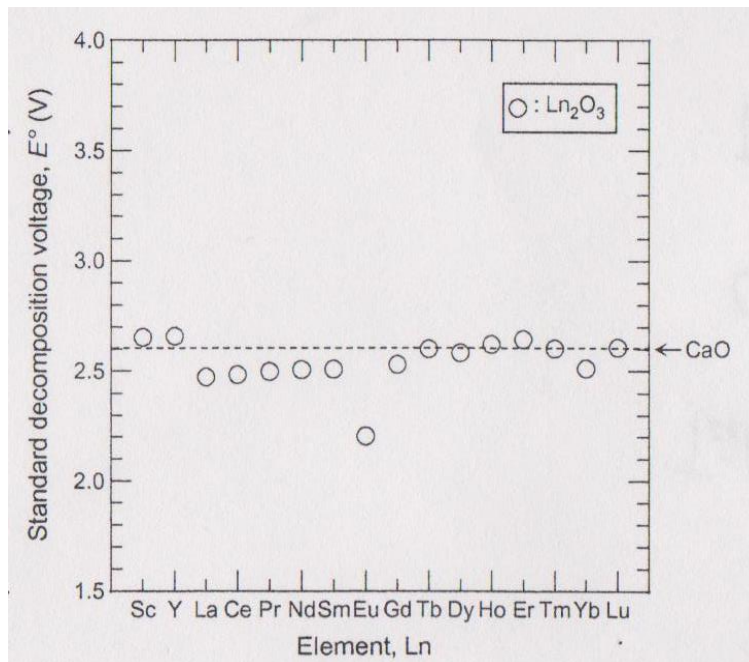


**Figure 8. Standard decomposition voltages of rare earth oxides at 1273°K (Osamu et al., 2014).**

Decomposition potential is influenced by temperature changes. Figures 9 and 10 mark out the decomposition potential of rare earth chlorides in chloride bath and rare earth fluorides in fluoride bath respectively with the variation of temperature.



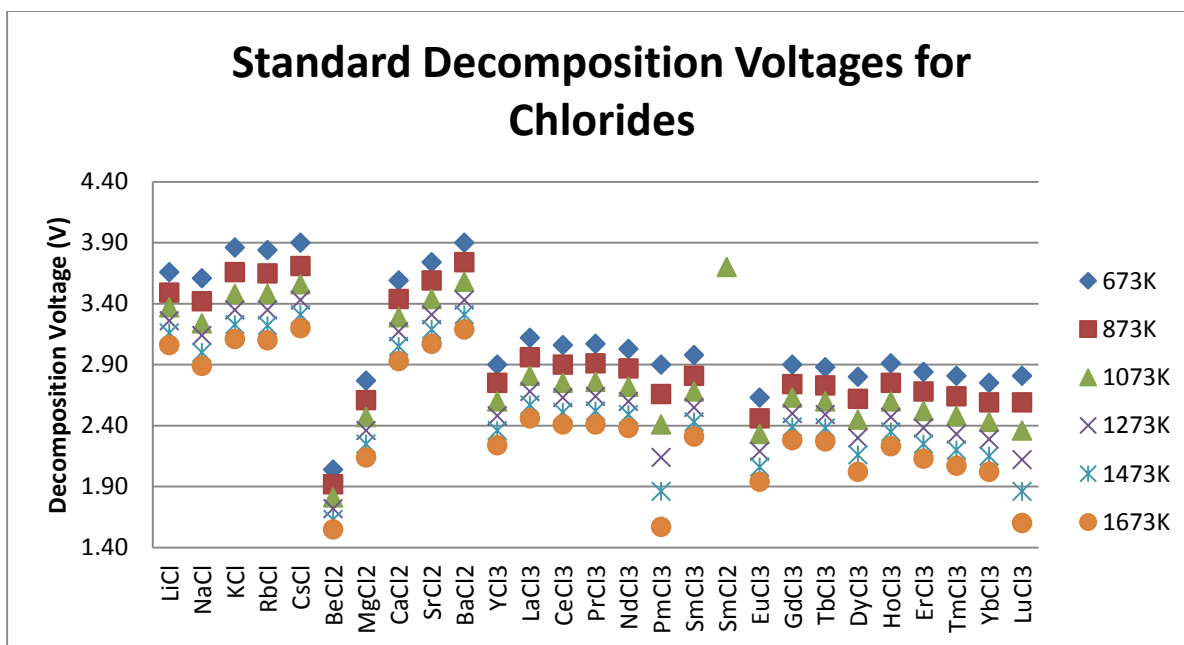


Figure 9. Standard decomposition voltage of rare earth chlorides and selected chloride salt

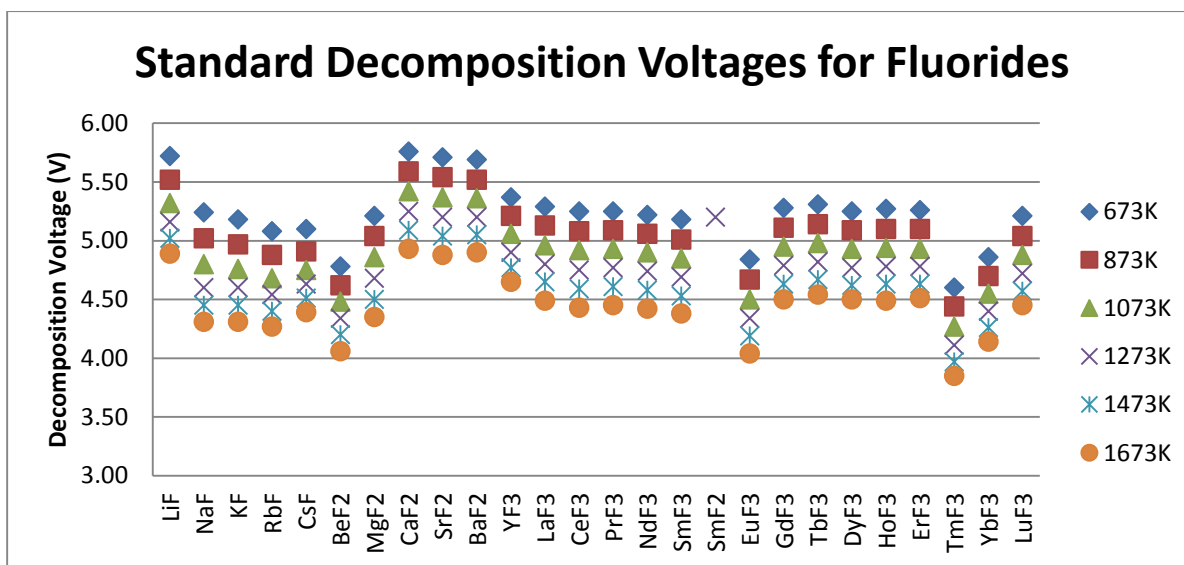


Figure 10. Standard decomposition voltage of rare earth fluorides and selected fluoride salt

Figure 9 and 10 include other elements besides rare earths such as: Li, Na, K, Cs, Be, and Mg. A few of those elements (Li, Ca, Sr, and Ba) have a higher decomposition voltage than most of rare earth compounds. This means that they are more stable and preferably used in the

electrolysis, because by having a low decomposition voltage of a fused salt, it will be easy to decompose, therefore, it will deposit in the cathode as impurities.

Both Figures 9 and 10 share the same value that with a lower temperature, decomposition potential will be higher. This means that it will require more potential (energy) for a compound to decompose at a lower temperature. In other words, a compound is more stable at lower temperature conditions. Comparing Figures 8, 9 and 10 show that the overall standard decomposition voltage rare earth in fluorides is higher than standard decomposition voltage rare earth chlorides and rare earth oxides, which is why the energy consumption in fluorides bath is higher (can be as high as 10kWh/kg). Nevertheless, rare earth oxide that is used as the raw feed normally has a less value of decomposition voltage, which can be seen in Table VI where the voltage used for rare earth oxide is lower than rare earth fluoride.

The presence of divalent rare earth is relatively very stable. It is detected that  $\text{SmCl}_2$  has the highest decomposition voltage ( $\sim 3.7\text{V}$ ) among others compound at  $1073^\circ\text{K}$  in Figure 9. At  $1273^\circ\text{K}$ ,  $\text{SmF}_2$  also has the highest value ( $\sim 5.2\text{V}$ ) compared with others compound in Figure 10 (Osamu et al., 2014). These confirm that the occurrence of divalent ions reduces the current efficiency due to the high stability that they exhibit, and it explains why samarium is not commercially produced using electrolysis at an industrial scale until now.

Results of electrolysis of rare earth can be seen in Table VI and Table VII. Table VI shows laboratory scale results of electrolysis in fluoride salt with particular voltage on each rare earth. To ensure all the rare earth decompose in the process, the operating voltage that is utilized on each rare earth is higher than the standard decomposition voltage. The current efficiency of samarium is equal to zero, that explains electrolysis of samarium in that condition is ineffective.

**Table VI. Results of electrolysis rare earth in laboratory scale using consumable anode (Osamu et al., 2014)**

| Product     | Cathode | Raw Material | Temp (°K) | Current (A) | Voltage (V) | Anode Consumption (%) | Current efficiency (%) |
|-------------|---------|--------------|-----------|-------------|-------------|-----------------------|------------------------|
| Y           | Ni      | Fluoride     | 1112      | 7.5         | 6.3         | 202                   | 67                     |
| La          | Ni      | Oxide        | 1127      | 4           | 2.8         | 249                   | 80                     |
| Ce          | Fe      | Fluoride     | 1082      | 9.4         | 3.8         | 26                    | 22                     |
| Pr          | Ni      | Fluoride     | 1108      | 4           | 7.5         | 147                   | 80                     |
| Pr          | Fe      | Fluoride     | 1106      | 5.9         | 6.7         | 240                   | 73                     |
| Nd-Pr       | Fe      | Fluoride     | 1113      | 5.2         | 6.5         | 184                   | 62                     |
| Nd-Pr       | Fe      | Fluoride     | 1108      | 5.9         | 6.3         | 171                   | 70                     |
| Nd-Dy       | Fe      | Fluoride     | 1148      | 5.5         | 9           | 142                   | 70                     |
| Sm          | Co      | Oxide        | 1177      | 4.4         | 3           | 146                   | 0                      |
| Sm          | Co      | Fluoride     | 1110      | 6.3         | 6.8         | 194                   | 0                      |
| Gd          | Fe      | Fluoride     | 1153      | 9.2         | 6           | 171                   | 58                     |
| Gd          | Co      | Fluoride     | 1104      | 8           | 6           | 173                   | 71                     |
| Gd-Tb       | Co      | Fluoride     | 1088      | 7.5         | 7.2         | 146                   | 79                     |
| Tb          | Fe      | Oxide        | 1211      | 4           | 2.5         | 236                   | 53                     |
| Tb          | Fe      | Fluoride     | 1174      | 6.2         | 6.4         | 89                    | 80                     |
| Tb          | Co      | Fluoride     | 1064      | 7.2         | 7.1         | 121                   | 59                     |
| Dy          | Fe      | Fluoride     | 1167      | 9.1         | 5.9         | 211                   | 59                     |
| Er          | Ni      | Fluoride     | 1172      | 8.9         | 5.4         | -                     | 55                     |
| Misch-metal | Ni      | Fluoride     | 1079      | 9           | 3.8         | 63                    | 31                     |

**Table VII. Results of electrolysis rare earth in industrial scale using consumable cathode (Osamu et al., 2014)**

| Type of electrolysis     | Rare earth oxide or fluoride in fluoride bath   |
|--------------------------|---|
| Product                  | Nd, Pr-Nd, Nd-Fe, Pr-Nd-Fe, Dy-Fe, Tb-Fe, Gd-Fe |
| Current                  | 1 - 30 kA                                       |
| Voltage                  | 8 - 15 V  |
| Cathode current density  | 0.3 - 3 A/cm <sup>2</sup>                       |
| Anode current density    | 0.5-30 A/cm <sup>2</sup>                        |
| Power consumption        | 7-12 kWh/kg Ln                                  |
| Current efficiency       | 80-90%  |
| Rare earth concentration | - Pure Ln: >99%<br>- Ln-Fe alloy: 78-88%        |

Table VII describes the electrolysis results for Nd, Pr-Nd, Dy-Fe, Pr-Nd-Fe, Tb-Fe, Gd-Fe at industrial scale which produce Ln with 99% purity and Ln-Fe alloy with 78-88% purity.

Some elements such as Mg, Al, Ca, C, and O can also be traced as impurities in the rare earth products of an electrolysis process.

### 3.5. Solubility

The solubility is the amount of a substance (solute) to dissolve in a solvent. Apparently, the solubility of rare earth oxides is really low, which hinders the electrolysis process efficiency. The solubility is mainly influenced by temperature and the solvent. As stated before, this paper will explain the solubility limited to rare earth oxides in fluoride melts. Nevertheless, it has a similar concept and approach for chloride melts.

#### 3.5.1. Temperature

Temperature plays an important role for the rare earth oxide solubility. The relation of rare earths' solubility and temperature in fluoride bath can be seen in Figure 11.

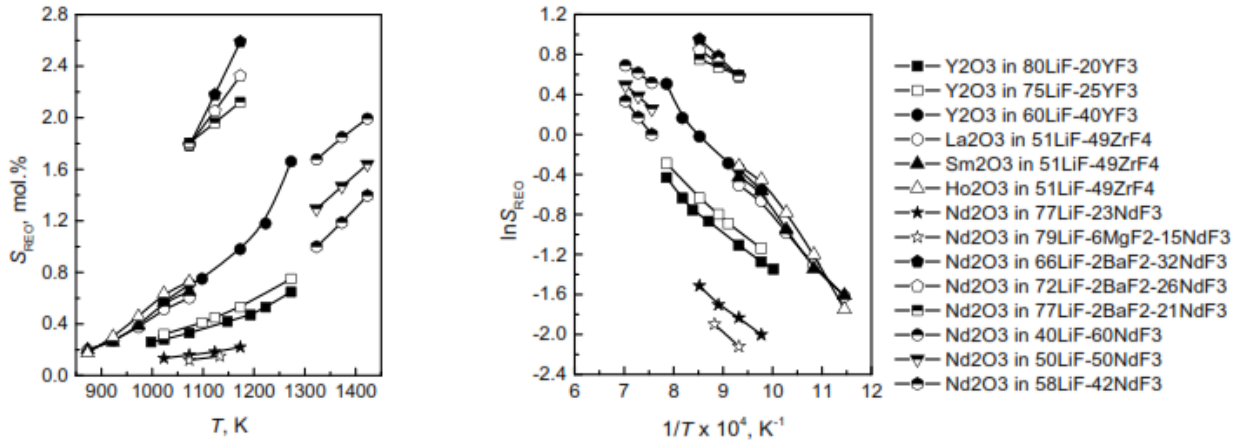


**Figure 11. Solubility of rare earth oxides in fluoride bath as a function of temperature**  
(Guo, Sietsma, & Yang, 2014)

Figure 11 depicts the solubility of Y, La, Sm, and Nd oxides in fluoride bath as a function of temperature. It also shows the reciprocal of the absolute temperature that is plotted against the logarithm of the rare earth solubility ( $\ln S$ ), which can be drawn from the equation:

$$\ln S_{REO} = a \times \frac{1}{T} + b \quad (11)$$

Where  $a$  and  $b$  are determined from the fitting parameters data plot that can be seen in Table VIII.

**Table VIII. Linear fitting parameters for data plots in Figure 11 (Guo, Sietsma, & Yang, 2014)**

| System  | R <sup>2</sup> | $a$ [10 <sup>3</sup> K] | $b$         |
|---|----------------|-------------------------|-------------|
| Y <sub>2</sub> O <sub>3</sub> in 80LiF-20YF <sub>3</sub>                        | 0.986          | -4.1 ± 0.2              | 2.7 ± 0.2   |
| Y <sub>2</sub> O <sub>3</sub> in 75LiF-25YF <sub>3</sub>                        | 0.991          | -4.4 ± 0.2              | 3.2 ± 0.2   |
| Y <sub>2</sub> O <sub>3</sub> in 60LiF-40YF <sub>3</sub>                        | 0.960          | -5.2 ± 0.5              | 4.5 ± 0.4   |
| La <sub>2</sub> O <sub>3</sub> in 51LiF-49ZrF <sub>4</sub>                      | 0.993          | -5.4 ± 0.2              | 4.5 ± 0.2   |
| Sm <sub>2</sub> O <sub>3</sub> in 51LiF-49ZrF <sub>4</sub>                      | 0.980          | -5.9 ± 0.4              | 5.1 ± 0.4   |
| Ho <sub>2</sub> O <sub>3</sub> in 51LiF-49ZrF <sub>4</sub>                      | 0.969          | -6.8 ± 0.6              | 6.2 ± 0.6   |
| Nd <sub>2</sub> O <sub>3</sub> in 77LiF-23NdF <sub>3</sub>                      | 0.987          | -3.8 ± 0.2              | 1.7 ± 0.2   |
| Nd <sub>2</sub> O <sub>3</sub> in 79LiF-6MgF <sub>2</sub> -15NdF <sub>3</sub> * | --             | -4.5213                 | 2.093       |
| Nd <sub>2</sub> O <sub>3</sub> in 66LiF-2BaF <sub>2</sub> -32NdF <sub>3</sub>   | 0.999          | -4.69 ± 0.08            | 4.96 ± 0.07 |
| Nd <sub>2</sub> O <sub>3</sub> in 72LiF-2BaF <sub>2</sub> -26NdF <sub>3</sub>   | 1.000          | -3.27 ± 0.01            | 3.63 ± 0.01 |
| Nd <sub>2</sub> O <sub>3</sub> in 77LiF-2BaF <sub>2</sub> -21NdF <sub>3</sub>   | 1.000          | -2.03 ± 0.02            | 2.48 ± 0.02 |
| Nd <sub>2</sub> O <sub>3</sub> in 40LiF-60NdF <sub>3</sub>                      | 0.994          | -3.3 ± 0.2              | 3.0 ± 0.1   |
| Nd <sub>2</sub> O <sub>3</sub> in 50LiF-50NdF <sub>3</sub>                      | 0.999          | -4.47 ± 0.08            | 3.64 ± 0.06 |
| Nd <sub>2</sub> O <sub>3</sub> in 58LiF-42NdF <sub>3</sub>                      | 1.000          | -6.29 ± 0.02            | 4.75 ± 0.01 |

\* with only two data

Table VIII shows that most rare earth oxides have R<sup>2</sup> value close to one (ideal). Nevertheless, these parameters are limited to a specific system and cannot be used to estimate the solubility of an unidentified system.

Figure 11 and equation 11 show that increasing temperature will increase the solubility of rare earth oxide. In addition, an endothermic reaction resulted (absorbing heat) during the dissolving process of rare earth oxide in solid state into a dissolved rare earth oxide.

### 3.5.2. Solvent content

#### 3.5.2.1. Rare earth fluoride and alkali metal fluoride content

Rare earth fluoride presence in a solvent of an electrolysis process is not only for extracting its rare earth, but it also helps to increase the solubility of rare earth oxide as the feed material. Figure 12 illustrates the solubility of rare earth oxides in fluoride bath with the

function of rare earth fluoride content. It concludes that the increasing of rare earth fluoride content will increase the solubility of the rare earth oxide.

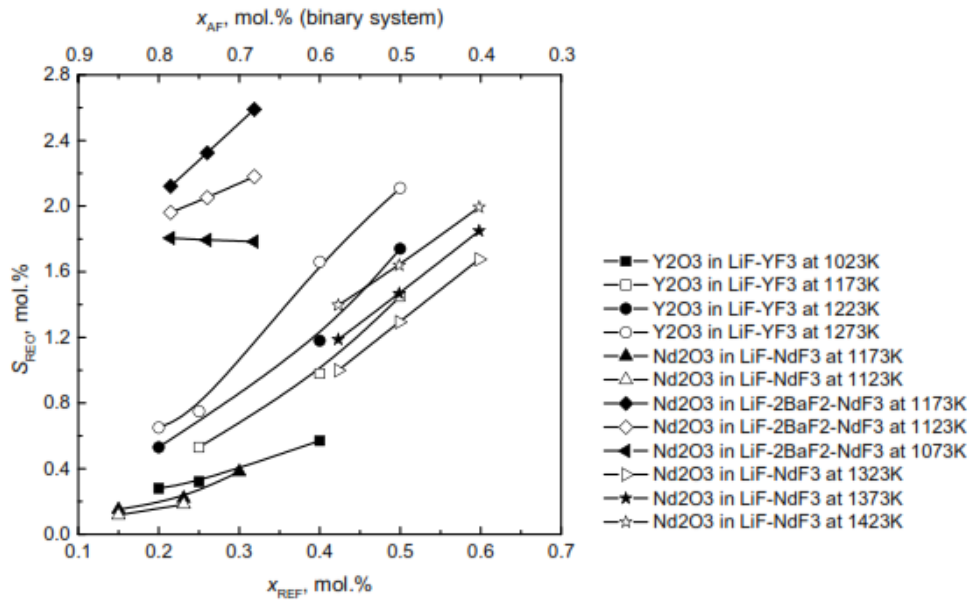


Figure 12. The solubility of rare earth oxides as a function of rare earth fluoride solvent content (Guo, Sietsma, & Yang, 2014)

Figure 12 shows the relationship of rare earth oxides' solubility with alkali metal content. It demonstrates that the presence of alkali metal oxide not only reduces the melting point of the rare earth oxide as it was stated previously, but it also has an adverse impact on the rare earth oxides' solubility. In other words, the higher alkali metal content will lower the solubility of the rare earth oxides.

### 3.5.2.2. Ionic radius

Ionic radius of the rare earths also influences the solubility of rare earth oxides. Figure 13 graphs the relation of ionic radius with the solubility. It illustrates that the solubilities increase as the ionic radius of  $\text{Ln}^{3+}$  decreases ( $S_{\text{Ho}_2\text{O}_3} > S_{\text{Sm}_2\text{O}_3} > S_{\text{La}_2\text{O}_3}$ ) and alkali metal cation radius in bath decreases as well ( $S_{\text{LiF}} > S_{\text{NaF}} > S_{\text{KF}}$ ). These results show that the electrolysis process is determined by the bonding between Ln-O, and between ions in the fluoride melt as well.

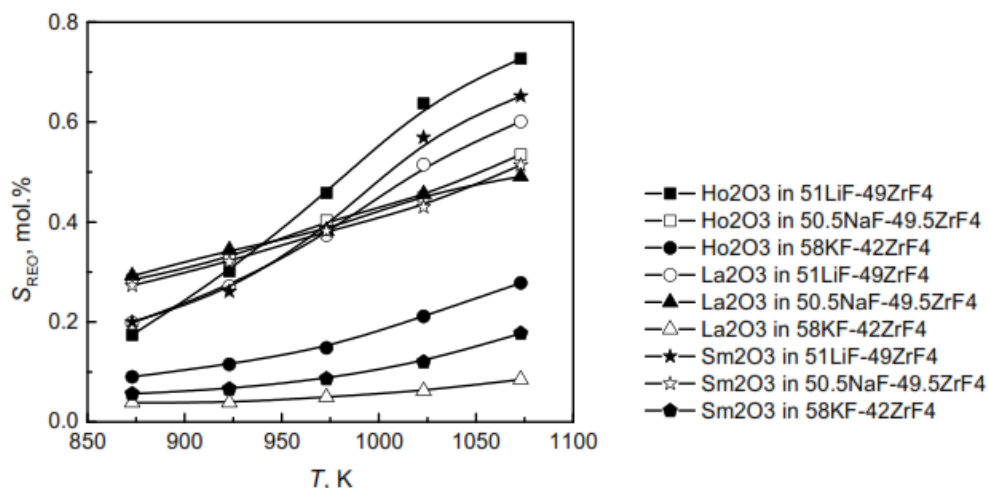


Figure 13. Solubility of Ho, La, and Sm as a function of temperature in fluoride melts (Guo, Sietsma, & Yang, 2014)

### 3.5.2.3. Alkali earth metal fluoride content

Adding alkali earth metal fluoride in the molten salt serves to lower the melting point of rare earth and lower the melt viscosity. Apparently, the solubility is not affected by the presence of alkali metal fluoride content. Figure 14 illustrates the Nd<sub>2</sub>O<sub>3</sub> solubility in LiF- alkali earth metal F<sub>2</sub>-NdF<sub>3</sub> as a function of alkali metal-F<sub>2</sub> addition.

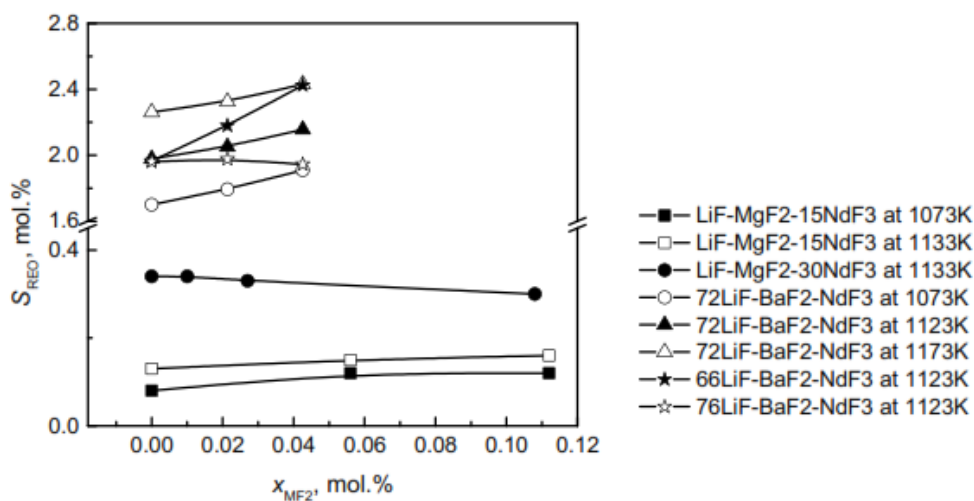


Figure 14. Solubility of Nd<sub>2</sub>O<sub>3</sub> solubility in LiF-Alkali Metal F<sub>2</sub> - NdF<sub>3</sub> (Guo, Sietsma, & Yang, 2014)

Figure 14 shows that as earth metal fluoride content increases, the solubility of rare earth oxides are relatively stable. In other words, the earth metal fluoride content does not affect the solubility of rare earth oxides.

### 3.6. E-pO<sup>2-</sup> Diagram

E-pO<sup>2-</sup> diagram is a diagram of the equilibrium potential (E) in a system that plotted against the activity of the oxide (pO<sup>2-</sup>) in the molten melt. This potential-pO<sup>2-</sup> diagram was first introduced by Littlewood (1960) to present the thermodynamics of molten salt systems using the similar concept of a Pourbaix diagram in an aqueous system. The major applications of this diagram have expanded not only for corrosion in the molten salt system (Jans & Timkins, 1979), but also for electrolytic reduction to active metals (Dring et al., 2005), which include the rare earth metals (Jiao & Zhu 2011).

#### 3.6.1. Comparison potential-pO<sup>2-</sup> with Eh-pH diagram

The limitation of the widely used Pourbaix diagram, a diagram of equilibrium potential against pH (Eh-pH) is that it works only in aqueous solutions, makes it inapplicable for electrolysis process of rare earth in molten salts which is operated at an elevated temperature. Nevertheless, E-pO<sup>2-</sup> diagram has a similar function as a Pourbaix diagram that purposely gives an understanding of the behavior of metals in contact with a system. The similarity and dissimilarity of both diagrams are best described by using an example of Fe systems (Chen, 1981).

Potential – pO<sup>2-</sup> diagram is reconstructed using the system described by Chen (1981) that used bath of NaNO<sub>3</sub> at 600°K and unit activities to both Fe<sup>2+</sup> and Fe<sup>3+</sup>. In comparison, the Eh-pH diagram was constructed at 298°K using databases from National Bureau Standards (Wagman,



1982) with  $\text{Fe}^{2+}$  and  $\text{Fe}^{3+}$  are the only dissolved species selected. Both system are respectively illustrated in E- $\text{pO}^{2-}$  and Eh-pH diagram on Figure 15 and 16.

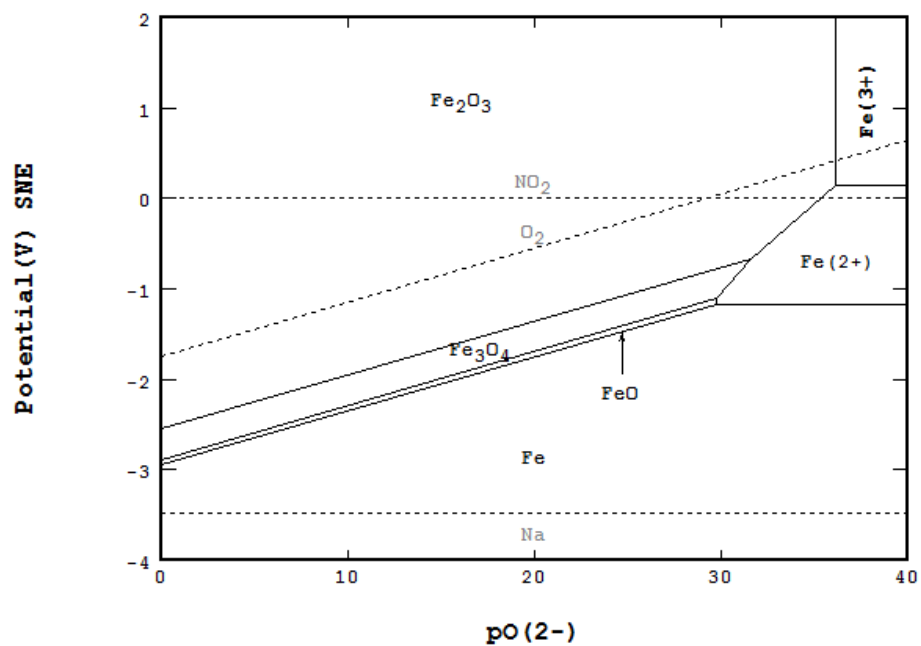


Figure 15. Potential- $\text{pO}^{2-}$  diagram of Fe in  $\text{NaNO}_3$  at  $600^\circ\text{K}$

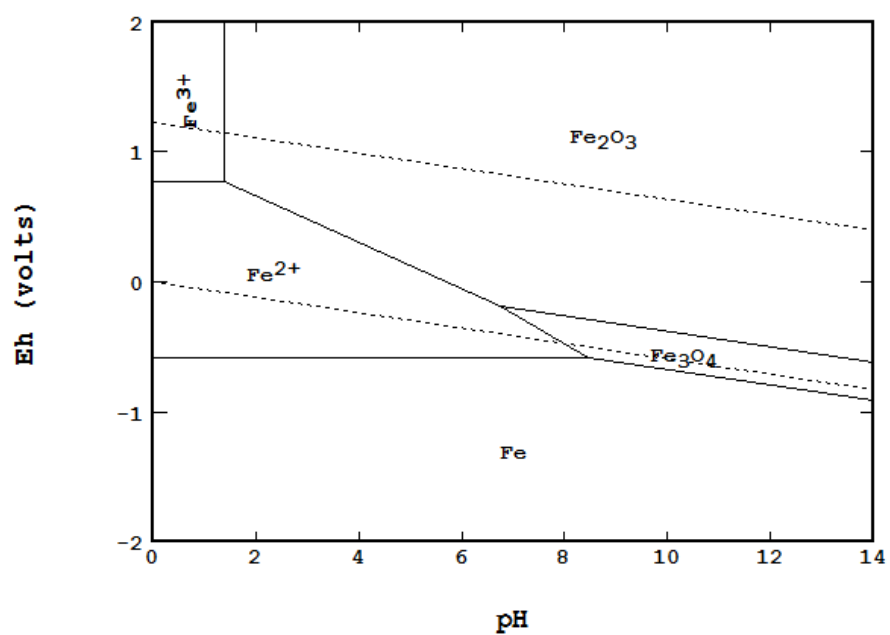


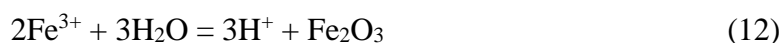
Figure 16. Eh-pH diagram of Fe in water at  $298^\circ\text{K}$

Both diagrams in Figure 15 and 16 have a similarity which is on the potential axis (Y-axis) that used for reduction potential. Both diagram also show the oxidized species occupy on the upper areas of the diagram, while the reduced species occupy the lower section of both diagrams. Nonetheless, besides that similarity, both diagrams have three main differences:

1. X- axis.

- The aqueous system uses  $H^+$  to separate acid and base of the metal acid =  $nH^+ +$

Base such as:



Since pH is defined as  $-\log(H^+)$ , acid species will be located on the low pH.

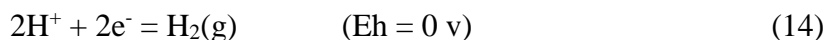
- The molten salt uses  $O^{2-}$  to separate acid and base (acid +  $mO^{2-}$  = base) such as:



$pO^{2-}$  is defined as  $-\log(O^{2-})$ , the acid species will be located on the high  $pO^{2-}$

2. Reference potentials.

-Reference potential ( $E_h = 0$  v) for an aqueous system, is standard hydrogen potential (SHE) as:



-Reference potential for molten salt is chosen either from anion or from cation.

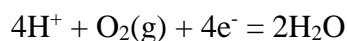
Anion is normally selected because there may be several different cations in the system. The bath for  $NaNO_3$  (anion) is used above. For instance  $NO_3^-/NO_2$  is selected as the reference potential ( $E = 0$  v).



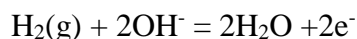
### 3. Stability area of the water and molten bath.

-For Eh-pH diagram, the stability area of water is stable within the two dashed lines, therefore on Figure 15:

- The upper stability is the formation from  $O_2(g)$ , i.e:

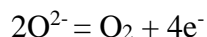


- The lower stability is the formation from  $H_2(g)$ , i.e:



-For molten diagram, the stability area of the bath depends on the salt itself, and can be seen from two dashed lines. Hence in Figure 16:

- The upper stability is labeled as  $NO_2$ , the formation reaction is:



- The lower stability is labeled as Na, the formation reaction is:



The differences of water and molten bath are summarized in Table IX.

**Table IX. Comparison of water and molten bath**

| Diagram                              | Eh-pH   | potential-pO <sup>2-</sup>  |
|--------------------------------------|---|---|
| <b>Bath</b>                          | H <sub>2</sub> O(l)   | Na-NO <sub>3</sub>  |
| <b>Major Ions</b>                    | H <sup>+</sup> and OH <sup>-</sup>  | Na <sup>+</sup> , NO <sub>3</sub> <sup>-</sup> and O <sup>2-</sup>                          |
| <b>Y-axis</b>                        | Potential (V)   | Potential (V)   |
| <b>X-axis, [species] = activity</b>  | pH = -log([H <sup>+</sup> ])  | pO <sup>2-</sup> = -log([O <sup>2-</sup> ])   |
| <b>Components added</b>              | Fe and O  | Fe and O  |
| <b>Species (metal and oxides)</b>    | Fe, FeO, Fe <sub>2</sub> O <sub>3</sub> and Fe <sub>3</sub> O <sub>4</sub>  | Fe, FeO, Fe <sub>2</sub> O <sub>3</sub> and Fe <sub>3</sub> O <sub>4</sub>                  |
| <b>Ionic Species</b>                 | Dissolved Fe <sup>2+</sup>  | Fe <sup>2+</sup> from dissolving Fe(NO <sub>3</sub> ) <sub>2</sub>                          |
|                                      | Dissolved Fe <sup>3+</sup>  | Fe <sup>3+</sup> from dissolving Fe(NO <sub>3</sub> ) <sub>3</sub>                          |
| <b>Reference potential V = 0</b>     | 2H <sup>+</sup> + 2e <sup>-</sup> = H <sub>2</sub> (g)                      | 2NO <sub>3</sub> <sup>-</sup> = 2NO <sub>2</sub> (g) + O <sub>2</sub> (g) + 2e <sup>-</sup> |
| <b>Stability of the bath (upper)</b> | 2H <sub>2</sub> O = 4H <sup>+</sup> + O <sub>2</sub> (g) + 4e <sup>-</sup>  | 2O <sup>2-</sup> = O <sub>2</sub> + 4e <sup>-</sup>   |
| <b>Stability of the bath (lower)</b> | 2H <sub>2</sub> O + 2e <sup>-</sup> = H <sub>2</sub> (g) + 2OH <sup>-</sup> | Na <sup>+</sup> + e <sup>-</sup> = Na   |
| <b>Range of Stability</b>            | 1.23V   | 3.5V  |

### 3.6.2. Acid and base (alkali) in molten salt

The basic concept of acid and base by Lewis stated that acids like to accept electrons, while bases like to give out electrons. The example of determining acid and base in an aqueous system can be seen in reaction 16:



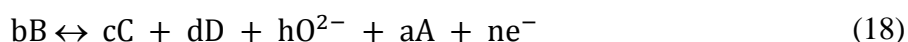
Species  $\text{Cu}^{2+}$  reacts as an acid because it receives electron for  $\text{OH}^-$  which is produced from  $\text{Cu}(\text{OH})^+$ . Same principle is applied to molten salt, for instance in reduction  $\text{SiO}_2$  in molten  $\text{CaCl}_2$  (Yasuda, 2007):



Species  $\text{SiO}_2(\text{s})$  is the acid, and  $\text{SiO}_3^{2-}$  dissolved in the bath dissociated from  $\text{CaSiO}_3$  is the base.

### 3.6.3. Equilibrium equations in molten salt system

The chemical equation between species A and B in the aqueous system with or without electron can be expressed as



Where, C and D are the ligands. Stoichiometric coefficient of a species will be positive if it is on the right hand side of the equation, and vice versa. Many equations and species are involved while performing the equilibrium calculation for an Eh-pH diagram, thus, it is easier to use standard free energy of formation of the species,  $dG^\circ$ . The first free energy of reaction can be calculated as:

$$dG_{\text{rex}} = \Sigma(v_i \times dG_i^\circ) \quad (19)$$

Where v represents the stoichiometric coefficient.

The equilibrium equations for the reaction with and without involving electrons (n) are:

1. Nernst equation for oxidation-reduction reaction

$$E = \left[ \frac{dG_{\text{rex}}}{(n \times F)} + \frac{\ln(10)RT}{(n \times F)} \times \log \left( \frac{\{A\}^a \{C\}^c \{D\}^d}{\{B\}^b} \right) \right] + \left( \frac{-h \times \ln(10)RT}{(n \times F)} \right) \times pO^{2-} \quad (20)$$

Where, R, T, and F are the gas constant (1.987 cal/mol), temp (°K), and Faraday constant (23060 cal/volt.equivalent). A, B, C, and D species are defined as the activities of species A, B, C, and D.

2. Non-Redox (electron) reaction:

$$pO^{2-} = \frac{1}{h} \times \left[ \log \left( \frac{\{A\}^a \{C\}^c \{D\}^d}{\{B\}^b} \right) + \frac{dG_{\text{rex}}}{\ln(10) \times RT} \right] \quad (21)$$

3. Neither electron nor  $H^+$  reaction:

$$\log Q - \log K = \log \left( \frac{\{A\}^a \{C\}^c \{D\}^d}{\{B\}^b} \right) + \frac{dG_{\text{rex}}}{\ln(10) \times RT} \quad (22)$$

Species B will be in favor if  $\log Q - \log K$  is positive, and vice versa.

#### 3.6.4. Application of the E- $pO^{2-}$ diagram for the metal reduction in the molten bath electrolysis

The reduction of  $La_2O_3$  as the raw feed in the molten chloride bath of NaCl:2CsCl at 873°K (600°C) was presented as an example based on S.Jiao, et al., (Jiao, 2004) experiment to implement and explain the use of E- $pO^{2-}$  diagram in the molten salt electrolysis process.

The E- $pO^{2-}$  diagram is constructed using the HSC databases (Roine, 2011) that is computed from the Nernst equation for oxidation-reduction reaction (equation 20), and modeled with STABCAL.

The diagram is a Pourbaix plot for the La-O system. The y-axis is labeled 'Potential (V) SCLE' and ranges from -5 to 1. The x-axis is labeled 'pO (2-)' and ranges from 0 to 50. The plot is divided into several regions by lines representing equilibrium between different phases. A vertical line at pO ≈ 18 separates the 'Base (more O<sup>2-</sup>)' region from the 'Acid (less O<sup>2-</sup>)' region. A horizontal line at V ≈ -2.9 separates the 'B' region (top) from the 'A' region (bottom). A diagonal line from (0, -5) to (18, 1) separates the 'La<sub>2</sub>O<sub>3</sub>' region from the 'LaOCl' region. A vertical line at pO ≈ 28 separates the 'LaOCl' region from the 'La (3+)' region. The 'La (3+)' region is shaded cyan. Labels include 'LaO<sub>2</sub> (g)' at the top left, 'La<sub>2</sub>O<sub>3</sub>' in the middle left, 'LaOCl' in the middle right, 'La (3+)' in the cyan region, 'La' in the bottom right, 'B' in the top right, and 'A' in the bottom right. A vertical double-headed arrow labeled 'Oxidation' and 'Reduction' is located in the 'La<sub>2</sub>O<sub>3</sub>' region. A horizontal double-headed arrow labeled 'Base (more O<sup>2-</sup>)' and 'Acid (less O<sup>2-</sup>)' is located at the bottom.

#### 3.6.4.1.1. Description of the X-axis and Y-axis in the E-pO<sup>2-</sup> diagram

Y-axis shows the potential (V, SC1E) that represents the voltage applied to or existent in the system. SC1E is the Standard Chloride Electrode which means the equilibrium voltage for the  $\text{Cl}_2(\text{g}) + 2\text{e}^- = 2\text{Cl}^-$  reaction, and has the value of 0 V defined as the standard (anion). If the standard reference selects the cation, which is Na in this case, the Standard Sodium Potential (SNaE) as the reference will be 0 V instead with the reaction of  $\text{Na}^+ + \text{e}^- = \text{Na}$ .

The X-axis uses the activity of oxide ion ( $pO^{2-} = -\log[O_2^-]$ ) that represents acid-base of the system. When a base chemical is added to a system, such as  $CaO = Ca^{2+} + O^{2-}$ , it will increase the concentration of  $O^{2-}$  and consequently decrease the value of  $pO^{2-}$ . In other words, CaO that contains more  $O^{2-}$  will be in the area of the low  $pO^{2-}$ .

#### 3.6.4.1.2. Distribution of La species on the E- $pO^{2-}$ diagram

In this selected system, there are many La species that complexed with  $O^{2-}$  and  $Cl^-$ . Lanthanum Chloride ( $LaCl_3$ ) dissociated in the chloride bath ( $LaCl_3 = La^{3+} + 3Cl^-$ ). Other compounds ( $La$ ,  $La_2O_3$ ,  $LaOCl$  and  $LaO_2(g)$ ) do not be dissolved but exist as solid or gas species. Nevertheless, the distribution of the species on the diagram depends on the potential and concentration of  $O^{2-}$ .

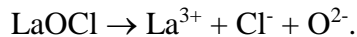
Figure 17 shows line-A and line-B. Line-A represents the equilibrium between La and  $La^{3+}$ . Since the valence (oxidation state) of  $La^{3+}$  is higher than La,  $La^{3+}$  will be located above La. Line-B represents the equilibrium between  $LaOCl$  and  $La^{3+}$ . Since  $LaOCl$  contains more  $O^{2-}$  compared to  $La^{3+}$ ,  $LaOCl$  will occupy the area on the left beside the  $La^{3+}$  and it will not be dissolved or decomposed to  $La^{3+}$ .

#### 3.6.4.1.3. The usage of the E- $pO^{2-}$ diagram to determine the reactions

The oxidation or reduction reaction in the E- $pO^{2-}$  diagram is determined by the species in the vertical direction. For instance, to produce La metal from  $La^{3+}$  species, the  $La^{3+}$  has to move down and across Line-A (downward), and the reduction reaction will be  $La^{3+} + 3e^- \rightarrow La$  metal. In short, the reduction reaction will go downward and the oxidation reaction will go upward.

The acid or base reaction in the E- $pO^{2-}$  diagram is determined by the species in the horizontal direction. For instance, to dissolve  $LaOCl$  species,  $LaOCl$  has to move to the right

direction and across Line-B (rightward). Hence, species  $\text{LaOCl}$  will lose  $\text{O}^{2-}$  with the reaction:



A system can also involve both oxidation-reduction and acid-base reactions, which require transfer of the species across a sloped line. For instance, Figure 15 shows a clear example of the  $\text{E-pO}^{2-}$  diagram of Fe in  $\text{NaNO}_3$  bath at  $600^\circ\text{C}$  that exhibit a slope line which separates  $\text{Fe}_2\text{O}_3$  and  $\text{Fe}^{2+}$ . The dissolution reaction in that system will be  $\text{Fe}_2\text{O}_3 + 2\text{e}^- \rightarrow 2\text{Fe}^{2+} + 3\text{O}^{2-}$ .

### 3.6.4.2. The $\text{E-pO}^{2-}$ diagram of La in chloride bath with additional electrolytic reactions

Figure 17 shows  $\text{E-pO}^{2-}$  diagram illustrates what will happen to La in the selected system. However, it requires another reactions to complete the whole process. Some basic reactions associated this La-Chloride system are shown as dashed lines on the following diagrams that can be seen in Figure 18.

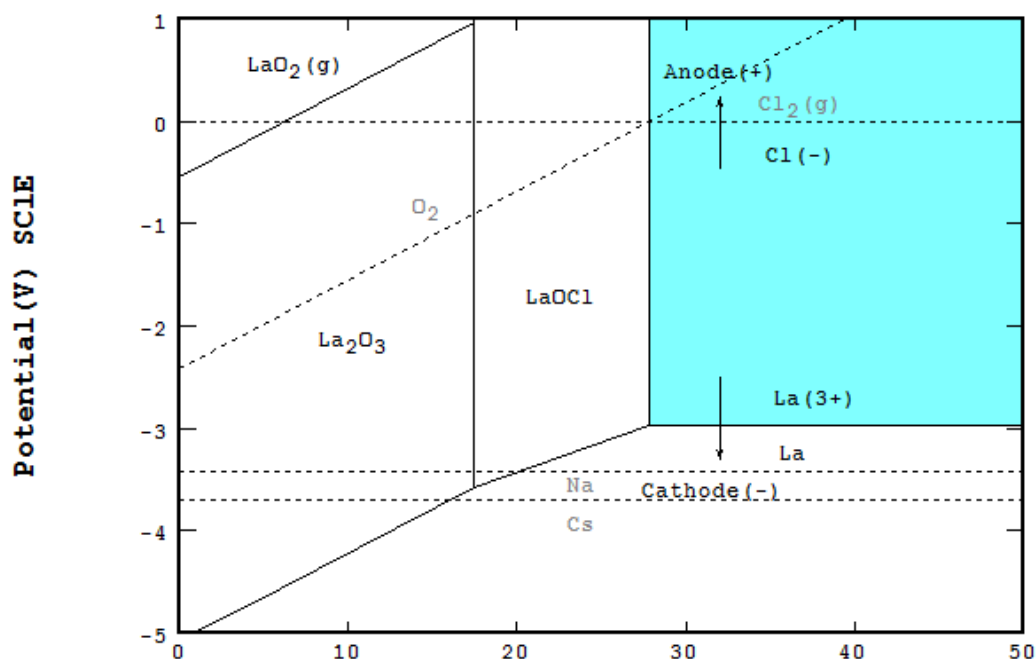


Figure 18.  $\text{E-pO}^{2-}$  diagram of La in the  $\text{NaCl:2CsCl}$  molten bath at  $600^\circ\text{C}$ . Stability of bath is shown by its decomposition potentials. The diagram also shows the potentials of anode and cathode reactions for extraction of La from the molten bath



#### 3.6.4.2.1. The stability of the chloride bath

Like a water, a molten bath can also be stable within a range of particular voltage and it depends on the composition of the bath which is best represented by the E-pO<sup>2-</sup> diagram. Since it is within a range, hence there will be two stability, upper and lower stability.

- The upper stability

The upper stability is the decomposition of the anion. In this selected chloride system (see Figure 18), the line is labeled as Cl<sub>2</sub>(g) on the graph. If above that line, the chloride ion in the molten bath will be oxidized to Cl<sub>2</sub>(g) with the reaction:  $2\text{Cl}^- (\text{bath}) = \text{Cl}_2(\text{g}) + 2\text{e}^-$ .

- The lower stability

The lower stability is the decomposition of the cations. In this NaCl:2CsCl system, two dash lines are labeled as Na and Cs (see Figure 18). If below the lines, the bath will be reduced to Na or Cs metals. Since Na line has a higher potential, it will be the first to be decomposed with the reaction:  $\text{Na}^+ (\text{bath}) + \text{e}^- = \text{Na}$ .

#### 3.6.4.2.2. Oxygen formation in the electrode

Since La<sub>2</sub>O<sub>3</sub> is fed to the selected system in the electrolytic cell, O<sub>2</sub> will be evolved in the anode. The overall reaction will be:  $2\text{La}_2\text{O}_3 \rightarrow 4\text{La}^{3+} + 6\text{O}^{2-} \rightarrow 4\text{La} (\text{metal at the cathode}) + 3\text{O}_2(\text{gas at the anode})$

#### 3.6.4.3. The electrolytic cell operation voltage (overall potential)

For the oxidation-reduction reactions to occur in this system, a few conditions should be met. At the cathode, the voltage should be lower than the equilibrium between  $\text{La}^{3+}$  and La with the reaction:  $\text{La}^{3+} + 3\text{e}^- \rightarrow \text{La}(\text{metal})$ . At the anode, the voltage should be higher than the equilibrium between  $\text{Cl}_2(\text{g})$  and  $\text{Cl}^-$  with the reaction:  $2\text{Cl}^- \rightarrow \text{Cl}_2(\text{g}) + 2\text{e}^-$ . Hence, by looking at Figure 18 diagram, the total applied voltage required should be greater than 3V, and the overall reaction will be:  $2\text{La}^{3+} + 6\text{Cl}^- \rightarrow 3\text{Cl}_2(\text{gas}) + 2\text{La}(\text{metal})$

#### 4. Implementing E-pO<sup>2-</sup> diagram for Nd<sub>2</sub>O<sub>3</sub> in LiF-NdF<sub>3</sub> system

Neodymium is one of the rare earth materials that is mainly used for permanent magnets (Nd-Fe-B). The development of electrolysis process has been replacing the metallothermic method for producing neodymium. This work will implement the E-pO<sup>2-</sup> diagram in an electrolysis of neodymium in a fluoride system. The conditions can be seen in Table X.

**Table X. Selected condition in a fluoride system for modeling E-pO<sup>2-</sup> diagram**

| Bath composition of LiF to NdF <sub>3</sub> | Mole % (75LiF to 25NdF <sub>3</sub> ) or weight % (28LiF to 72NdF <sub>3</sub> ) |
|---|--|
| Temperature                                 | 750°C (1023.15°K)  |
| Solubility                                  | 0.13 mole %  |
| Databases                                   | Kubaschewski (Kubaschewski, 1993) and HSC (Roine, 2012)                          |
| Reference electrode                         | $2F^- = F_2(g) + 2e^-$   |
| Cathode                                     | Non-Consumable tungsten  |
| Anode                                       | Consumable carbon  |

This bath composition is chosen according to the binary diagram of LiF with NdF<sub>3</sub>, that does not form a complex compound compare with KF-NdF<sub>3</sub> and NaF-NdF<sub>3</sub> (See Figure 17). Furthermore, LiF has a higher decomposition potential than the KF and NaF which make LiF more stable and desirable. According to Stefanidaki, Hasiotis & Kontoyannis (2001), LiF can also increase the fluidity, while in NaF bath, the complex fluoride compound of NaNdF<sub>4</sub> can be formed and increase the viscosity which will decrease the effectiveness process in the electrolysis.

LiF and  $\text{NdF}_3$  system have a lowest melting point ( $\sim 720^\circ\text{C}$ ) at composition around 25mole% $\text{NdF}_3$  and 75mole%LiF (see Figure 19). Temperature of  $750^\circ\text{C}$  or  $1023.15^\circ\text{K}$  is selected to ensure all the molten salt is maintained in the liquid state.

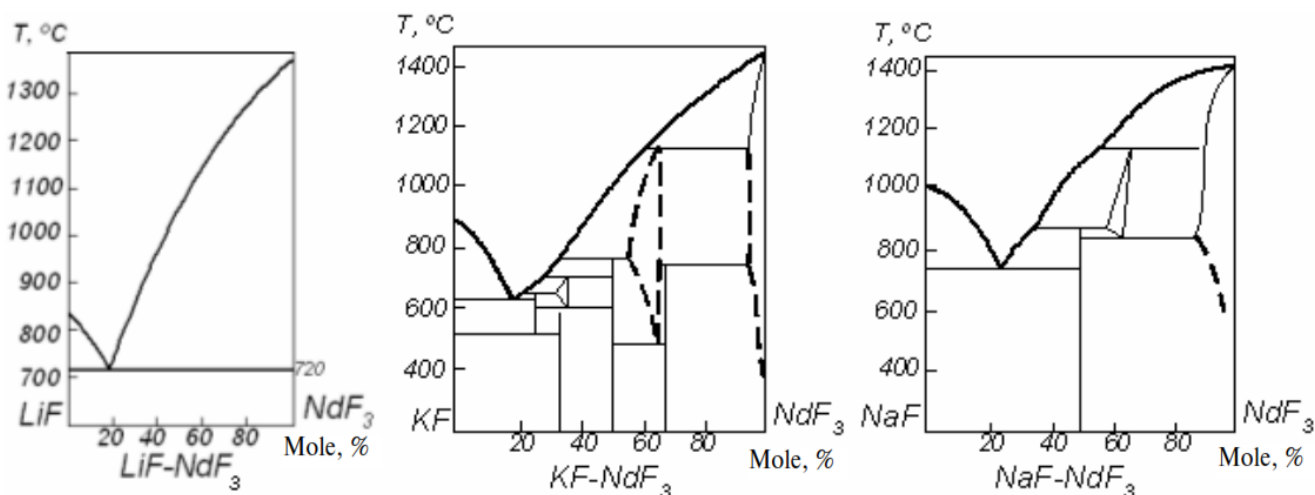


Figure 19. Binary diagram of  $\text{NdF}_3$  with alkali metal fluoride (Grebnev and Dmitrienko, 2007)

#### 4.1. Databases of HSC and Kubaschewski

The free energies of formation of relevant species at  $1023.15^\circ\text{K}$  can be found in equation 19. This work will select two databases (see Table VIII) from Kubaschewski (Kubaschewski, 1993) and HSC (Roine, 2011). Species fluoride ( $\text{F}^-$ ) and electron ( $\text{e}^-$ ) are ionic species in molten bath.  $\text{dG}$  of  $\text{F}^-$  will be zero, because  $\text{F}_2(\text{g})/\text{F}^-$  is chosen to be the reference electrode. Table XI shows the tabulated free energies formation of the selected condition.

**Table XI. Free energies formation of Nd in LiF<sub>3</sub> and NdF<sub>3</sub> at 1023.15°K**

| Databases                      | HSC      | Kubaschewski |
|--------------------------------|----------|--------------|
| Species                        | dG(kcal) | dG (kcal)    |
| e <sup>-</sup>                 | 0        | 0            |
| F <sup>-</sup>                 | 0        | 0            |
| F <sub>2</sub> (g)             | 0        | 0            |
| C(Graphite)                    | 0        | 0            |
| Nd                             | 0        | 0            |
| O <sub>2</sub> (g)             | 0        | 0            |
| Li                             | 0        | 0            |
| LiF                            | -121.451 | -123.295     |
| Li <sup>+</sup>                | -121.451 | -123.295     |
| Li <sub>2</sub> O              | -110.389 | -110.577     |
| NdF <sub>3</sub>               | -341.662 | -348.281     |
| Nd <sup>3+</sup>               | -341.662 | -348.281     |
| Nd <sub>2</sub> O <sub>3</sub> | -363.066 | -363.139     |
| CO(g)                          | -48.404  | -48.3354     |
| CO <sub>2</sub> (g)            | -94.6174 | -94.6432     |
| O <sup>2-</sup>                | 267.6888 | 278.149      |

Note: dG of Li<sup>+</sup> and Nd<sup>3+</sup> come from the dissociation of metal fluorides in the molten bath,

for instance:  $\text{NdF}_3(\text{s}) = \text{Nd}^{3+} + 3\text{F}^-$ .

## 4.2. Modeling E-pO<sup>2-</sup> diagram with STABCAL

STABCAL is a program developed by Dr. Hsin-Hsiung Huang that presents stability calculation for chemical systems. This program can construct different types of stability diagrams such as: Ellingham diagram, Pourbaix diagram, and E-pO<sup>2-</sup> diagram, etc. STABCAL's program layout can be seen in STABCAL start menu, shown in Figure 20. As for the databases, STABCAL has several Gibbs free energy (dG) databases such as: NBS (Wagman, 1982), MINTEQ (visual minteq), Maumov (Russia), Kubaschewski (Kubachewski, 1993), HSC (Roine, 2011) and others.

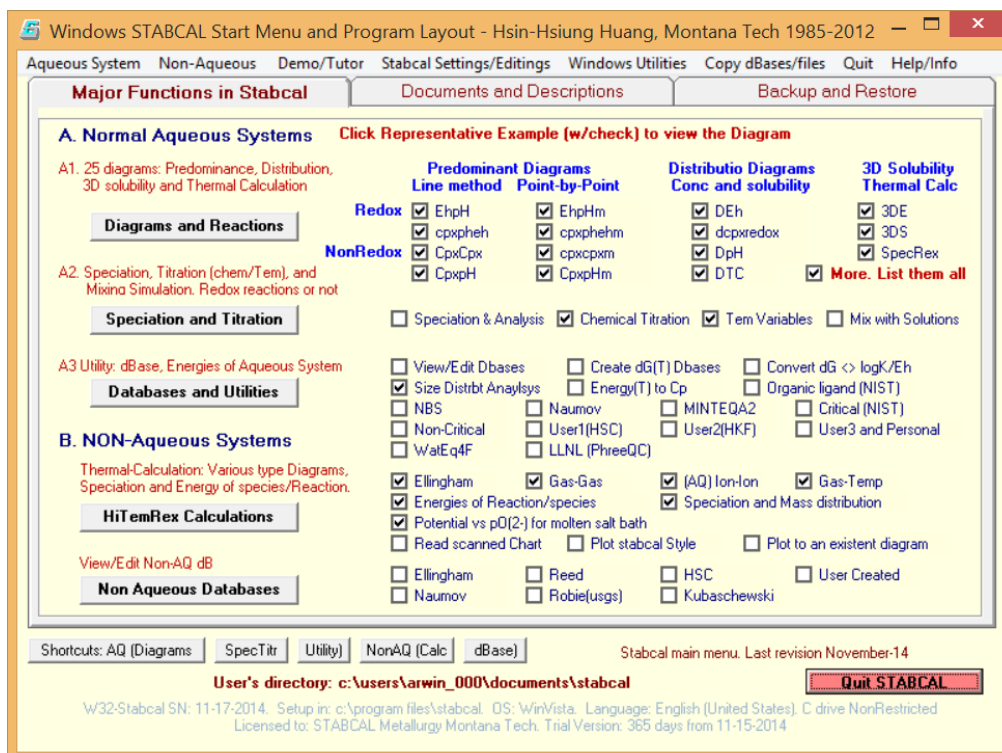


**Figure 20. STABCAL's Interface**

## 5. Results and Discussion

### 5.1. Reactions and potential $\text{Nd}_2\text{O}_3$ in $\text{LiF-NdF}_3$ system

Reactions and line equations for E- $\text{pO}^{2-}$  diagram that occur in the electrolysis of  $\text{Nd}_2\text{O}_3$  in  $\text{LiF-NdF}_3$  system with its tabulated potential are (showed as solid lines in Figure 21 and 22):



$$\text{HSC: Potential} = -4.97936 \quad \text{Kubaschewski: Potential} = -5.07504$$



$$\text{HSC: pO}^{2-} = 34.9360 \quad \text{Kubaschewski: pO}^{2-} = 36.23356$$



$$\text{HSC: Potential} = -8.52570 + 0.101508\text{pO}^{2-}$$

$$\text{Kubaschewski: Potential} = -8.75302 + 0.101508\text{pO}^{2-}$$



$$\text{HSC: Potential} = -6.85354 + 0.101508\text{pO}^{2-}$$

$$\text{Kubaschewski: Potential} = -7.07885 + 0.101508\text{pO}^{2-}$$


---

As for electrodes, reactions and line equations for E- $\text{pO}^{2-}$  diagram with its potential are (showed as dashed lines in Figure 19 and 20):



$$\text{HSC: Potential} = 0 \quad \text{Kubaschewski: Potential} = 0$$



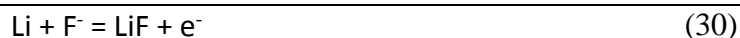
$$\text{HSC: Potential} = -5.80404 + 0.101508\text{pO}^{2-}$$

$$\text{Kubaschewski: potential} = -6.03084 + 0.101508\text{pO}^{2-}$$


---



HSC: Potential = -4.93862    Kubaschewski: Potential = -5.0343



HSC: Potential = -5.26659    Kubaschewski: Potential = -5.34659

---

The results above are computed by STABCAL based from the Nernst reduction-oxidation equation (equation 20), and the potential results are showing similar values between HSC and Kubaschewski databases, which can also be shown in Figure 21 and 22.

## 5.2. E-pO<sup>2-</sup> diagram of Nd<sub>2</sub>O<sub>3</sub> in LiF-NdF<sub>3</sub> system

E-pO<sup>2-</sup> diagram of Nd<sub>2</sub>O<sub>3</sub> in mole% 75LiF - mole% 25NdF<sub>3</sub> is shown in Figure 21 and 22.

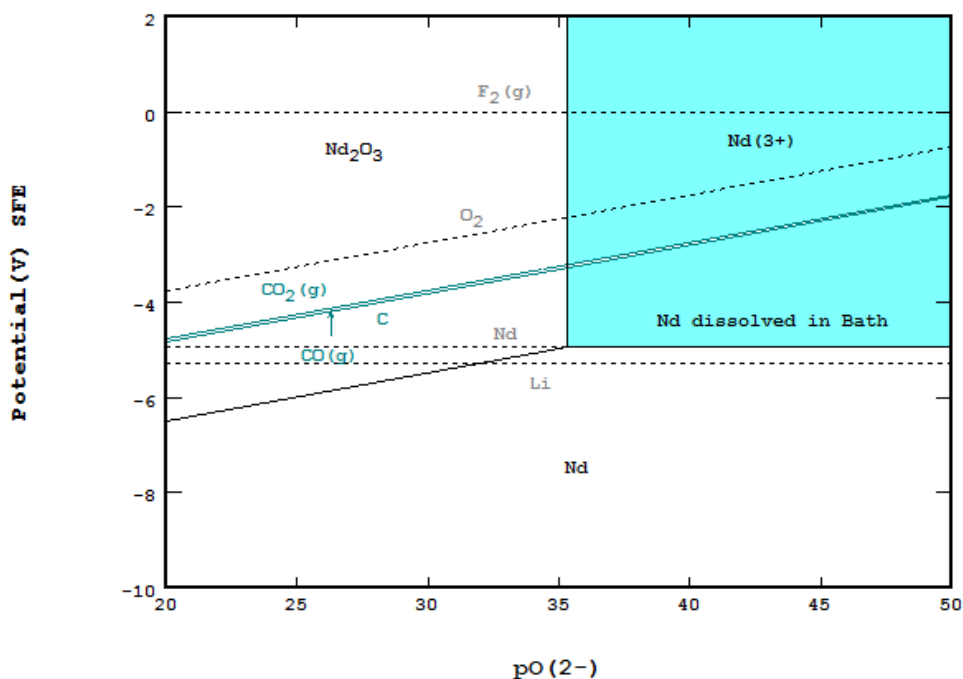


Figure 21. E-pO<sup>2-</sup> diagram of Nd<sub>2</sub>O<sub>3</sub> in mole% 75LiF - mole%25 NdF<sub>3</sub> at 1023.15°K (HSC databases)



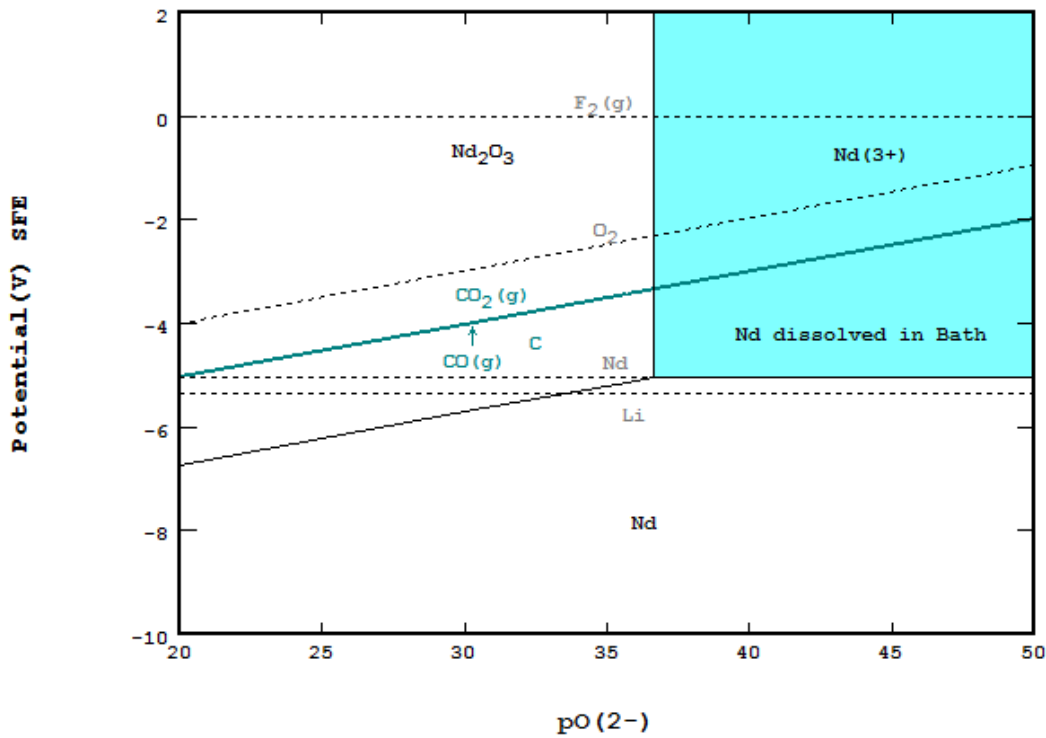


Figure 22. E- $pO^{2-}$  diagram of  $Nd_2O_3$  in mole%75 LiF - mole%25  $NdF_3$  at 1023.15°K (Kubaschewski databases)

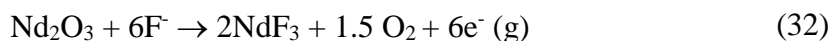
Both figures show the similar trend and diagram using HSC (Figure 21) and Kubaschewski (Figure 22), therefore they share the same function. That diagram describes that the range potential of the Nd metal (shown in dash line,  $V = -5.075V$ ) to reference is higher than the range potential Li metal (shown in dash line,  $V = -5.345V$ ) to reference. Hence, Li is more stable than Nd, which makes decomposition of Nd to the cathode is more viable.

Due to the low solubility of the  $Nd_2O_3$  oxide, which is less than 0.2% solubility (Stefanidaki et al., 2001), the area of interest should be as close as possible to the boundary line between  $Nd^{3+}$  and  $Nd_2O_3$ , where the  $pO^{2-}$  is close to 35 (HSC) or 36 (Kubaschewski).

Based on the cyclic voltammetry studies conducted by Stefanidaki et al., (2001), they proposed the overall cathode reaction was the deposition of Nd metal as:



Judging from the diagram, the equilibrium voltage is around -5V (-5.08V from Kubaschewski, and -4.98V from HSC). In the anode, formation of  $O_2(g)$  will be produced and will be reacted further with carbon. The reactions that occur in the anode are:



Equilibrium potential formation of oxygen can be varied depending on the activity of the oxide ion ( $pO^{2-}$ ). The equilibrium potential for formation of oxygen will be close to -2.5 V at  $pO^{2-} = 35$  (HSC) and -1.0V at  $pO^{2-} = 50$ .

Assuming 0.5V of over voltage is applied to each equilibrium voltages, the voltage to the cathode will be -5.5V (more negative), which value is within the voltage used by Grebnev and Dmitrienko (2007) experiment that has practical value of 4 to 8 total voltage. As for the anode voltage (towards positive), the potential required will be -2.0V to make the oxidation reaction occur. Hence, the theoretical cell voltages will be the difference between the anode and the cathode voltage that is 3.5V. This example is illustrated in Figure 23.

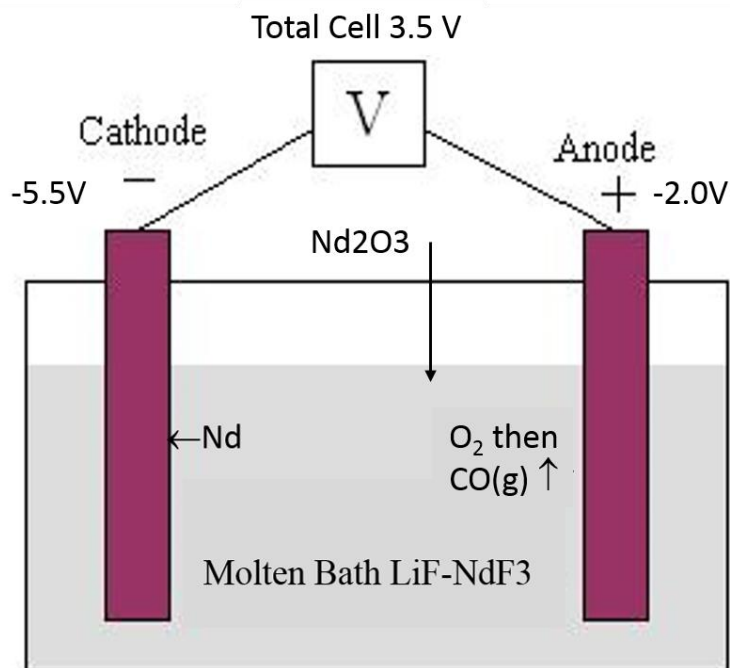


Figure 23. Electrolysis of Nd in fluoride system illustration.

### 5.3. Decomposition Competition between Nd and Li Metals

When a bath contains more than one type of metal ions, equilibrium potential between metal ion and metal ( $E_{\text{equilibrium}}$ ) plays an important role in determining which metal will be extracted. The criteria is cathodic overvoltage ( $\eta = E_{\text{equilibrium}} - E_{\text{applied}}$ ). The highest overvoltage will be the dominant reaction. Figure 24 shows a magnification of E-pO<sup>2</sup> diagram result with the addition of LiF formation.

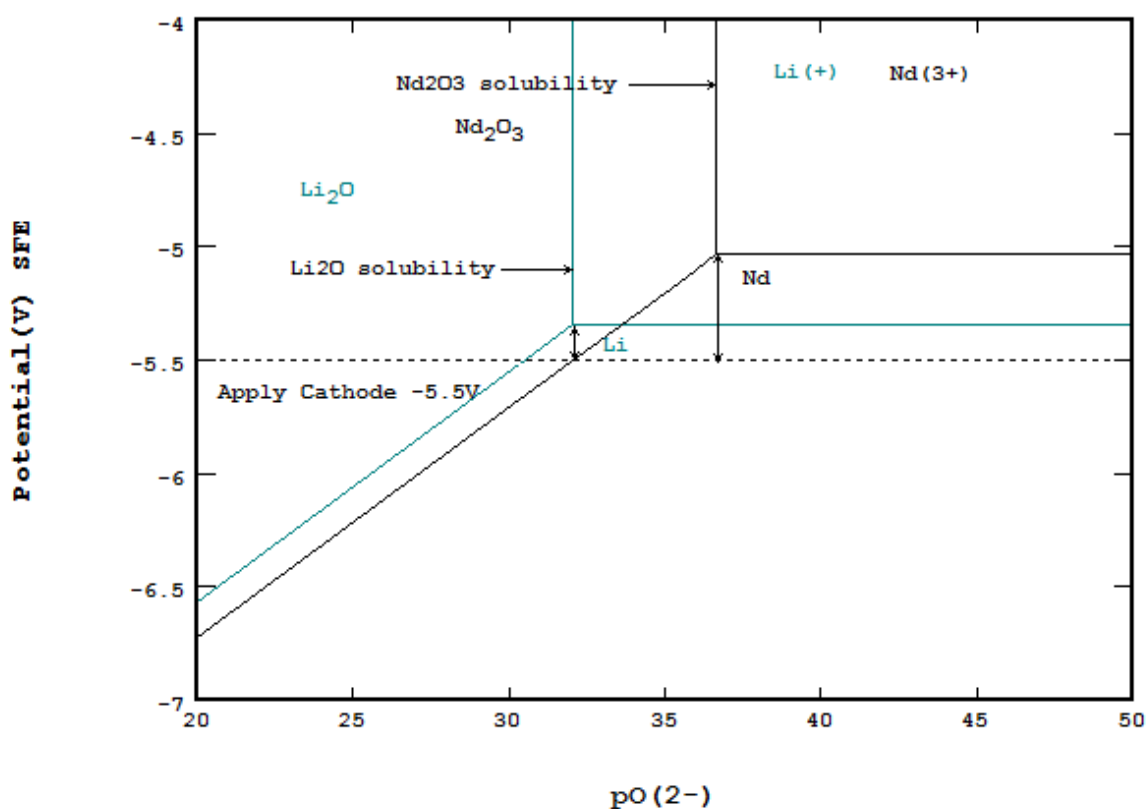


Figure 24. E-pO<sup>2</sup> diagram of Nd<sub>2</sub>O<sub>3</sub> with additional formation of LiF potential.

The diagram is merged from Nd and Li systems in the same molten bath. The diagram is focused on the cathodic area, and assuming the applied cathode voltage to be -5.5V. The cathodic overvoltage will be 0.425V for Nd and 0.153V for Li. Therefore, the amount of Nd<sup>3+</sup> decomposed to metal Nd in the cathode is greater than Li<sup>3+</sup> (higher driving force).

## 6. Conclusion

Extracting rare earths using molten salt electrolysis is not an easy task due to the rare earths' characteristics which are extremely stable. However, by understanding thermodynamic considerations, an optimum result can be achieved. There are several essential factors that need to be concerned such as: molten salt, decomposition potential, solubility and rare earth properties.

In a molten salt system, by having a combination of molten salt as a solvent, it can reduce the high operating condition in molten salt electrolysis (lower melting point). Moreover, it can help increase the solubility of rare earth oxide as the feed. Chloride molten salt is more economical compared to fluoride bath due to lower melting point of the rare earth chloride compounds compared to fluoride compounds. Nevertheless, chloride molten salt has a lower current efficiency compared to fluoride molten salt, due to high hygroscopicity and the presence of divalent ion rare earths, which are stable in the chloride system. An exception is found in divalent ion of samarium (Sm), that is stable in both chloride and fluoride bath.

While the metallothermic process considers standard Gibbs energy formation as the basis in extracting rare earths, electrolysis considers decomposition potential. Decomposition potential of rare earth in chloride and fluoride compounds are high, which make them really hard to decompose. Few molten salts like Li, Ca, and Sr have higher decomposition potential than rare earths compound, which are more desirable.

The solubility of rare earth oxides are really low. The solubility can be affected by temperature, where higher temperature will increase the solubility. Adding rare earth fluoride as a solvent in the fluoride bath electrolysis can help increase the solubility of the rare earth oxide.

Alkali metal fluoride showed an adverse effect on the solubility of rare earth oxide, while alkali earth metal fluoride did not affect the solubility in the fluoride bath.

E-pO<sup>2-</sup> diagram can be modeled and implemented in electrolysis of rare earth. E-pO<sup>2-</sup> diagram for Nd in 75mole% LiF - 25mole% NdF<sub>3</sub> at 1023.15°K, has shown decomposition voltage about 5 volt (HSC and Kubaschewski databases), which is between the range of the voltage (4-8 volt) used by V.A. Grebnev and V.P. Dmitrienko (2007) in a similar condition. In this system, the graph (Figure 24) shows that Nd metal is more in favor to form in the cathode, because of overvoltage, which can determine whether Nd or Li metal will be deposited in the cathode, is greater. Since overvoltage of Nd (0.425V) is greater than Li (0.153V), hence Nd metal will be extracted in the cathode (higher driving force).

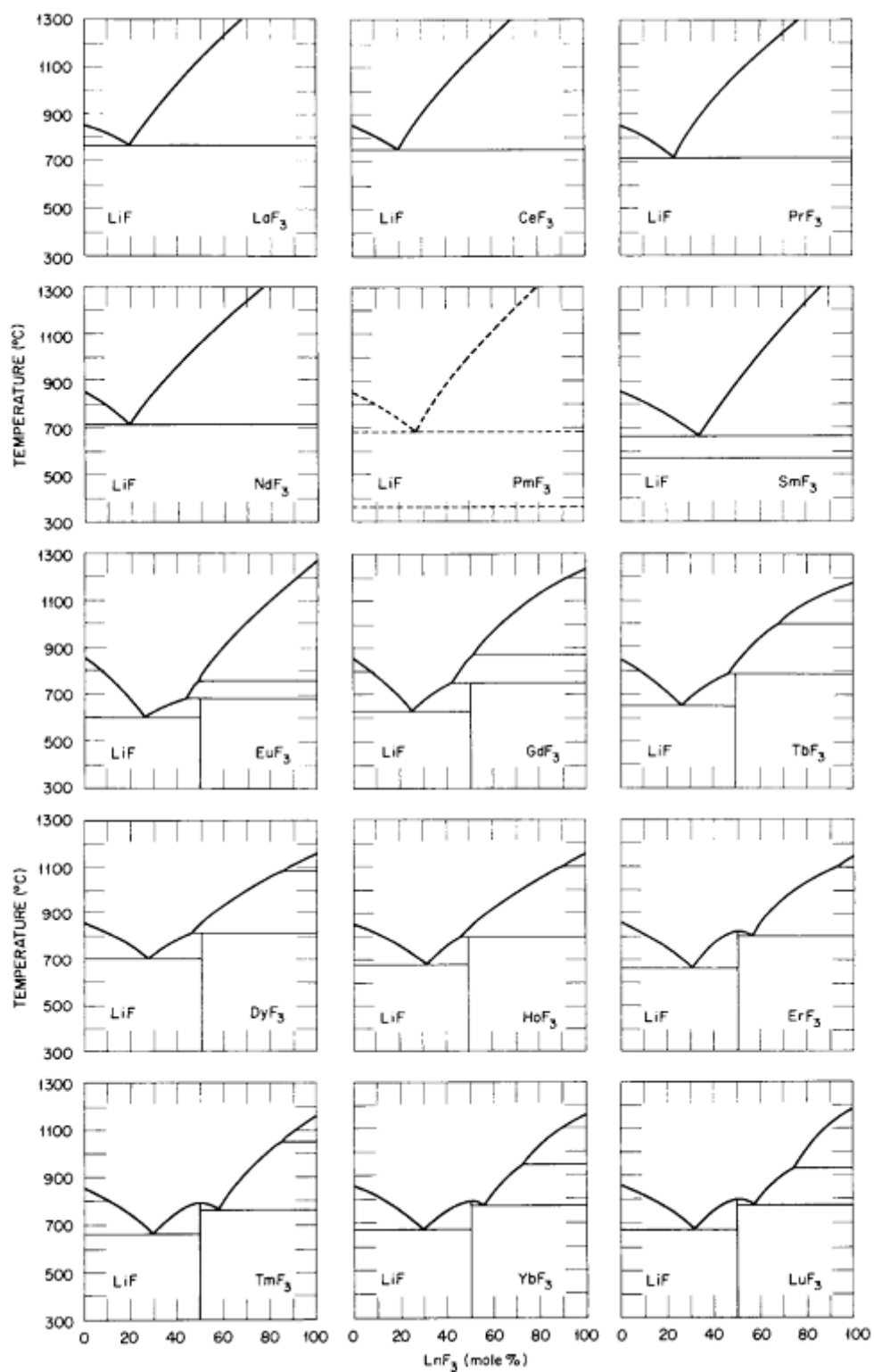
## References Cited

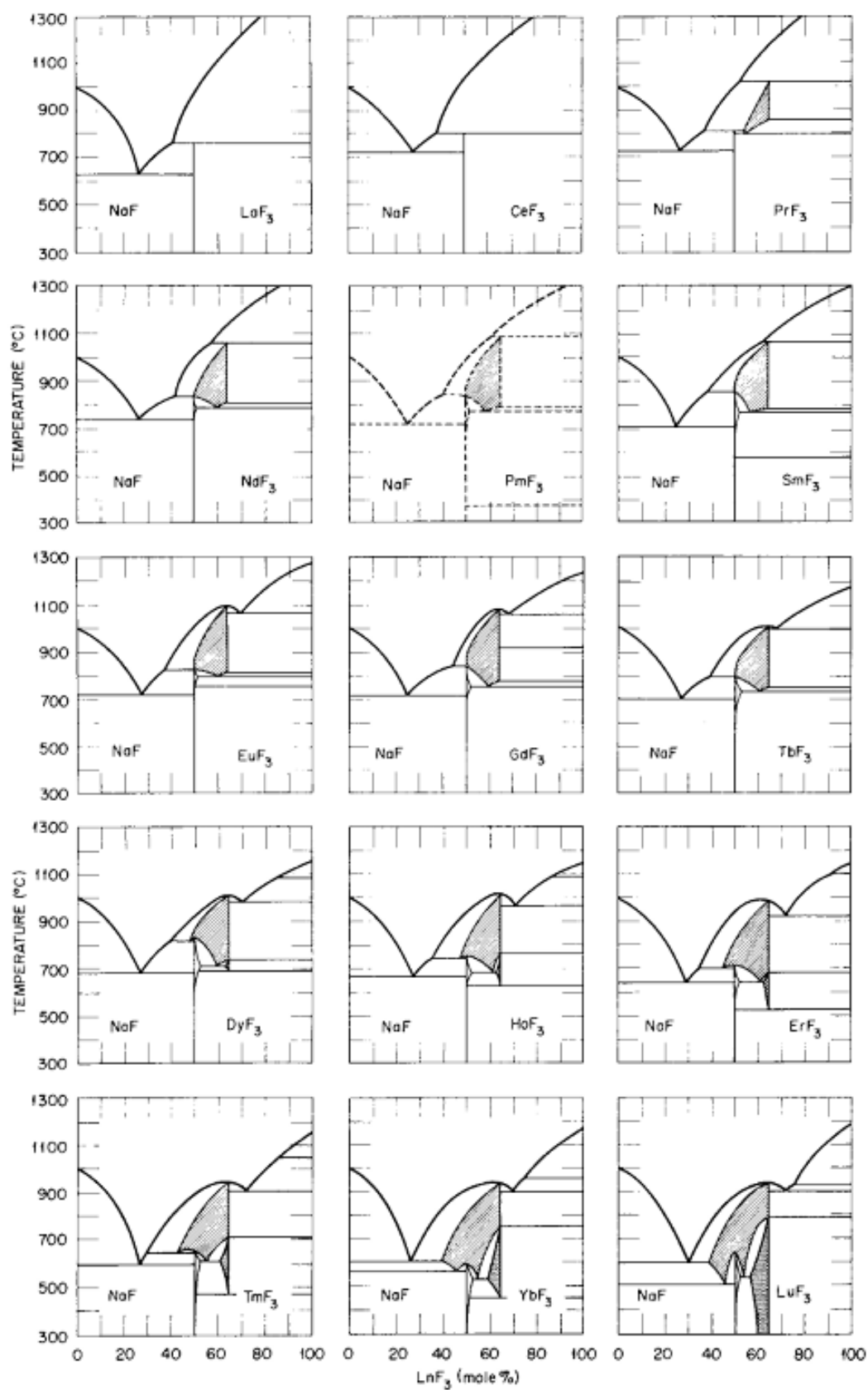
1. Gupta, C.K. (2005). *Extractive Metallurgy of Rare Earths*. Boca Raton: CRC Press.
2. U.S. Environmental Protection Agency. (2012). *A Review of Production, Processing, Recycling, and Associated Environmental Issues*. Cincinnati, OH.
3. Cotton, S.A. (2006). *Lanthanide and Actinide Chemistry*. Rutland, UK: John Wiley & Sons, Ltd.
4. Oak Ridge National Laboratory. (1963). *Mixtures of Metals with Molten Salts* (20th ed., Rev). Washington D.C: U.S. Government Printing Office.
5. Edeleanu C. & Littlewood R. (1960). *Thermodynamics of Corrosion in Fused Chloride system*, *Electrochimica Acta*, Vol 3, 195-207.
6. Brajendra, M., & David, L.O. (2004) *Molten salt applications in materials processing*.
7. Fact Sage. (2015). [Graph illustration the binary diagram of KBr-KF]. *A Mixture of Molten Salt*. Retrieved from [http://www.crct.polymtl.ca/fact/phase\\_diagram.php?file=KBr-KF.jpg&dir=FTsalt](http://www.crct.polymtl.ca/fact/phase_diagram.php?file=KBr-KF.jpg&dir=FTsalt)
8. Thoma, R.E. (1965). *Rare-Earth Halides*. Tennessee, TN: Oak Ridge National Laboratory.
9. Zhu, H. (2014). *Rare Earth Metal Production by Molten Salt Electrolysis*, 1765-1772.
10. Takeda, O., Uda, T., & Okabe, T.H. (2014). *Rare Earth, Titanium Group Metals, and Reactive Metals Production*, Vol 3, 995-1004.
11. Stefanidaki, E., Hasiotis, C., & Kontoyannis C. (2001). *Electrodeposition of neodymium from LiF-NdF<sub>3</sub>-Nd<sub>2</sub>O<sub>3</sub> melts* - *Electrochimica Acta*, Vol 46, 2665-2670.
12. Morrice, E., Wyche, C., & Henrie, T.A. (1962). *Electrowinning of molten lanthanum from lanthanum oxides*, *Bureau of Mines Report of Investigations 6075*, U.S. Department of the Interior, Washington, D.C.

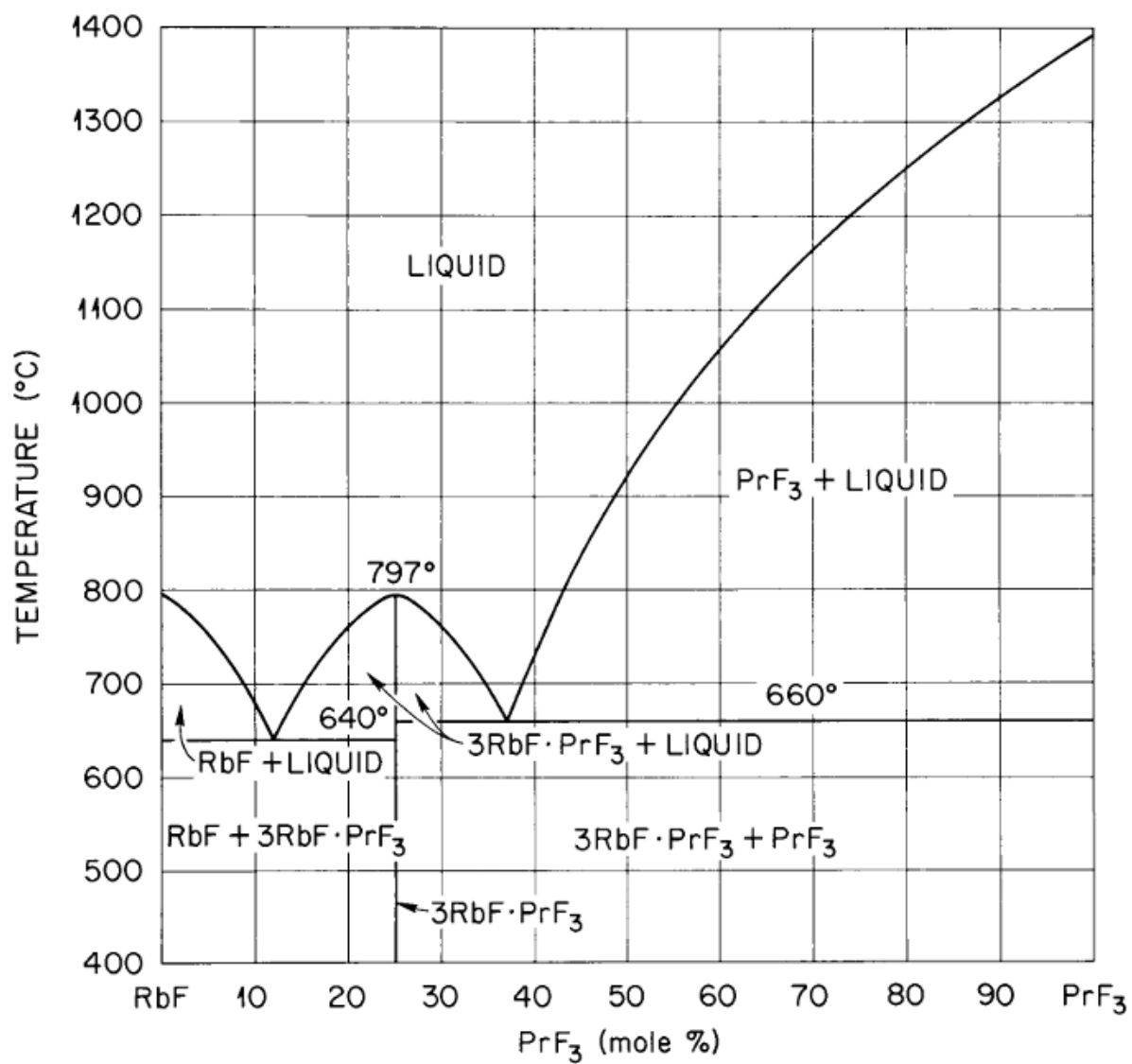
13. Boghosian, S., Papatheodorou, G.N., Gschneidner Jr., K.A., & Eyring, L. (1996), *Handbook on the Physics and Chemistry of Rare Earths*, Amsterdam, p. 435.
14. Guo, X., Sietsma, J., & Yang, Y. (2014). *Solubility of Rare Earth Oxides in Molten Fluorides: 1st European Rare Earth Resources Conference*. Milos, Greece.
15. Janz G.J. & Tomkins R.P.T. (1979). *Corrosion in Molten Salts: An Annotated Bibliography*  
*Corrosion – The Journal of Science and Engineering*, Vol 35 486-504.
16. Dring K., Dashwood R. & Inman D. (2005). *Predominance Diagrams for Electrochemical Reduction of Titanium Oxides in Molten  $\text{CaCl}_2$* , J. of Electrochemical Society, Vol 152, D184-190.
17. Jiao S. & Zhu H. (2011). *An investigation into the Electrochemical Recovery of Rare Earth Ions in a CsCl-based Molten Salt*, Journal of Hazardous Materials, Vol 189, 821-826.
18. Chen C.M. & Theus G. J. (1981). *Electrochemical Behavior of Carbon Steel Fused Salt*,  
Electrochemical Corrosion Testing ASTM STP 727, 303-326.
19. O. Kubaschewski, et. al. (1993). *Materials Thermo-chemistry*, Sixth edition, Pergamon Press.
20. A. Roine. (2012). *Outokumpu HSC Chemistry for Window*. Version 7.
21. K. Yasuda, T. Nohira, R. Hagiwara & Y.H. Ogata. (2007). *Diagrammatic Representation of Direct Electrolytic Reduction of  $\text{SiO}_2$  in Molten  $\text{CaCl}_2$* , J. Electrochemical Society, 154 (7) E95-E101.
22. D.D. Wagman, et. al. (1982). *The NBS tables of chemical thermodynamic properties*, J. of Physical and Chemical References Data, Vol. 11, Sup. 2, and Errata. Vol. 18(1989).

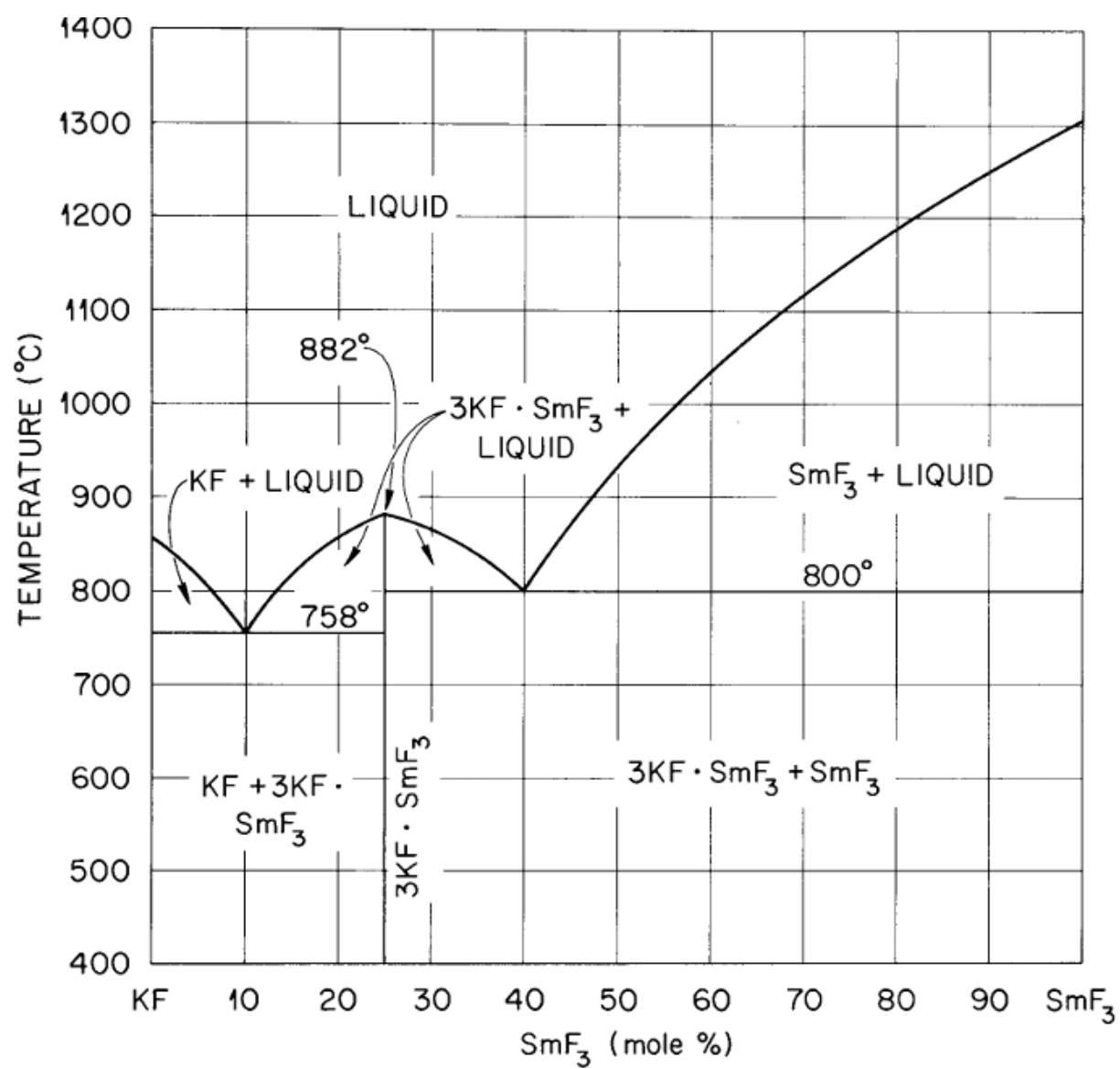


## Appendix A: Binary phase diagrams of rare earths in fluoride system (Thoma, 1965)



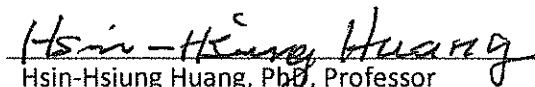




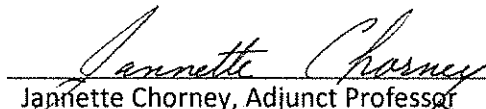


## SIGNATURE PAGE

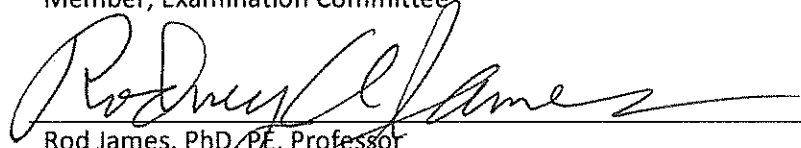
This is to certify that the thesis prepared by Arwin Gunawan entitled "Thermodynamic Considerations in Molten Salt Electrolysis for Rare Earth Metals" has been examined and approved for acceptance by the Department of Metallurgical & Materials Engineering, Montana Tech of The University of Montana, on this 11th day of May, 2015.



Hsin-Hsiung Huang, PhD, Professor  
Department of Metallurgical & Materials Engineering  
Chair, Examination Committee



Jannette Chorney, Adjunct Professor  
Department of Metallurgical & Materials Engineering  
Member, Examination Committee



Rod James, PhD, PE, Professor  
Department of Environmental Engineering  
Member, Examination Committee